Charles University in Prague
Faculty of Mathematics and Physics

DOCTORAL THESIS

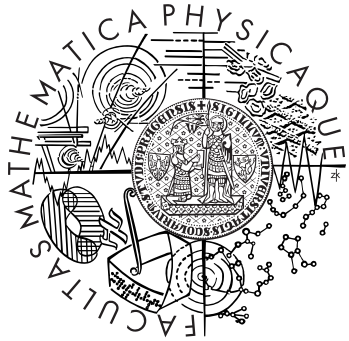

Kateřina Helisová

Models for random union of interacting discs

Department of Probability and Mathematical Statistics

Supervisor: Prof. RNDr. Viktor Beneš, DrSc.
Field of study: Probability and Mathematical Statistics

I would like to thank to my supervisor Prof. RNDr. Viktor Beneš, DrSc., and to Prof. Jesper Møller, D.Sc. (Aalborg University, Denmark) for their help and useful comments during the preparation of this work. Further, I thank to Jan Šimek and Jakub Staněk for their helpful suggestions and remarks to the software solution.

I declare that this thesis was written by myself and using the quoted references. I agree with using this thesis for study purposes.

In Prague, 17^{th} June 2009

Kateřina Helisová

Contents

Title: Models for random union of interacting discs
Author: Kateřina Helisová
Department: Department of Probability and Mathematical Statistics
Author's e-mail address: helisova@karlin.mff.cuni.cz
Supervisor: Prof. RNDr. Viktor Beneš, DrSc.
Supervisor's e-mail address: benesv@karlin.mff.cuni.cz
Consultant: Prof. Jesper Møller, D.Sc.
Consultant's e-mail address: jm@math.aau.dk

Abstract: A flexible class of finite disc process models with interactions among the discs is studied. Let $\mathcal{U}$ denote the random set given by the union of discs. For the disc process, an exponential family density with the statistics depending only on geometric properties of $\mathcal{U}$ (e.g. the area, perimeter, Euler-Poincaré characteristic or number of holes) is used. Viewing the model as a connected component Markov point process becomes useful for handling the problem with edge effects when $\mathcal{U}$ is observed only within a bounded observation window. The power tessellation and its dual graph become major tools when establishing inclusion-exclusion formulae and formulae for computing geometric characteristics of $\mathcal{U}$. First, stability properties of the density and algorithms for constructing the power tessellation of $\mathcal{U}$ and for simulating the disc process are discussed. Secondly, methods for estimating the parameters and other statistical inference are introduced, especially, it is shown how edge effects and other complications can be handled by considering a conditional and unconditional likelihood. The methodology is then illustrated by analyzing Peter Diggle's heather dataset, where the results of simulation-based maximum likelihood inference and the effect of specifying different reference Boolean models are discussed. Finally, software solution for simulations and for statistical inference is described.

Keywords: Boolean model, disc process, edge effects, exponential family, germ-grain model, inclusion-exclusion formulae, interaction, local stability, Markov properties, point process, power tessellation, random closed set, Ruelle stability, shape characteristics, simulation-based maximum likelihood, summary statistics.

Chapter 1

Introduction

Many phenomena in nature form a random set. As examples, we can introduce grows of trees or bushes, infected cells on flowers or in bodies etc. The most of them can be described by a germ-grain model

$$\mathbf{X} = \cup_{i=1}^{\infty}(u_i + \mathbf{K}_i) = \cup_{i=1}^{\infty}(\{u_i + y : y \in \mathbf{K}_i\}),$$

where $\mathbf{K}_i$ (the grains) are random compact subsets of $\mathbb{R}^d,\ d = 2, 3$, and their translations u_i (the germs) form a point process.

The random closed set $\mathcal{U}$ considered in this work is a germ-grain model with the grains being discs. The basic random-disc process models are random-disc Boolean models which play the main role in practice. The Boolean model is given by a Poisson process of the grains with no interaction among them. However in practice, the grains do not need to be independent, but they may mutually interact, and therefore developing flexible germ-grain models with interaction among the grains is also needed.

We study a model with interactions among the discs specified by a density of a disc process $\mathbf{X}$ with respect to a reference Boolean model. The density is assumed to be of exponential family form, with the statistic $T(\mathbf{X}) = T(\mathcal{U})$ depending on $\mathbf{X}$ only through the whole union $\mathcal{U}$, where $T(\mathcal{U})$ is specified in terms of geometric characteristics for the connected components of $\mathcal{U}$, for example the area $A(\mathcal{U})$, the perimeter $L(\mathcal{U})$, the number of holes $N_{\mathrm{h}}(\mathcal{U})$, the number of connected components $N_{\mathrm{cc}}(\mathcal{U})$ etc. Further geometric characteristics are specified in Section 3.3 in terms of the power tessellation which provides a subdivision of $\mathcal{U}$ (see Figure 3.1 in Section 3.2).

An important special case of our models is the quermass-interaction process, first introduced in [11], where $T(\mathcal{U}) = (A(\mathcal{U}), L(\mathcal{U}), \chi(\mathcal{U}))$ and $\chi(\mathcal{U}) = N_{\mathrm{cc}}(\mathcal{U}) - N_{\mathrm{h}}(\mathcal{U})$ is the Euler-Poincaré characteristic. Another special case is then the continuum random cluster model (see [9]), where $T(\mathcal{U}) = N_{\mathrm{cc}}(\mathcal{U})$.

The model is then illustrated by analyzing Peter Diggle's heather data (see [4]) which previously have been modeled by a Boolean model, however, it was noticed that it does not describe the data well, while - as shown in this work - our model provide obvious improvement.

The work is organized as follows:

In Chapter 2, there are introduced some basic definitions and relations used in the work.

Chapter 3 which follows from the paper [14], describes the model and then concerns the theoretical results as Ruelle and local stability of the density, formulae for computing geometric characteristics of $\mathcal{U}$ and Markov properties. Except this, there is defined the power tessellation and its dual graph and shown their usefulness for deriving some of the results and also for calculations carried in MCMC algorithm for simulating $\mathbf{X}$ which is described at the end of the chapter.

Various statistical methods and their applications for the model published also in [15] are shown in Chapter 4. There are given solutions to some basic problems such as edge effects or unobservable grains which usually occur when doing statistical analysis of spatial data, accenting how Markov properties of $\mathbf{X}$ become useful. Consequently, estimates of the density parameters are obtained and suitability of the model with that parameters is checked.

Finally, in Chapter 5, the program for simulating the model from a given density and the programs for estimating the parameters and for model validation are described.

Chapter 2

Basic definitions and notation

2.1 Point processes

Definition 2.1 *Let $(\Omega, \mathcal{F}, P)$ be a probability space. Consider $\mathcal{N}$ the system of locally finite subsets of $\mathbb{R}^d$ with the σ-algebra $\mathfrak{N} = \sigma(\{\mathbf{x} \in \mathcal{N} : \sharp(\mathbf{x} \cap A) = m\} : A \in \mathcal{B}, m \in \mathbb{N}_0)$, where $\mathcal{B}$ denotes a bounded Borel sets. A* point process *X defined on $\mathbb{R}^d$ is a measurable mapping from $(\Omega, \mathcal{F})$ to $(\mathcal{N}, \mathfrak{N})$.*

Definition 2.2 *The* distribution *P_X of a point process X is given by the relation $P_X(F) = P(\{\omega \in \Omega : X(\omega) \in F\})$ for $F \in \mathfrak{N}$.*

Definition 2.3 *A locally finite diffusion measure Λ on $\mathcal{B}$ satisfying $\Lambda(A) = \mathbb{E}X(A)$ for all $A \in \mathcal{B}$ is called the* intensity measure. *If there exists a function $\rho(x)$ for $x \in \mathbb{R}^d$ such that the intensity measure $\Lambda(A) = \int_A \rho(x)dx$, then $\rho(x)$ is called the* intensity function. *If the intensity function $\rho(x)$ is constant, $\rho(x) = \rho$, the point process is called* homogeneous with the intensity ρ. *Else it is said to be* inhomogeneous.

Definition 2.4 *A point process is called a* finite point process *if the intensity measure $\Lambda(\mathbb{R}^d) < \infty$.*

Definition 2.5 *A point process X is* stationary *if its distribution is invariant under translation, i.e. for all $v \in \mathbb{R}^d$, the distribution of $X + v = \{u + v, u \in X\}$ is the same as that of X.*
A point process X is isotropic *if its distribution is invariant under rotation.*
If a point process is both stationary and isotropic, it is called motion invariant.

Definition 2.6 *The* Poisson point process Y *is the process which satisfies:*

- *for any finite collection* $\{A_n\}$ *of disjoint sets in* $\mathbb{R}^d$*, the numbers of points in these sets,* $Y(A_n)$*, are independent random variables,*
- *for each* $A \subset \mathbb{R}^d$ *such that* $\Lambda(A) < \infty$*,* $Y(A)$ *has Poisson distribution with parameter* $\Lambda(A)$*, i.e.* $P[Y(A) = k] = \frac{\Lambda(A)^k}{k!} e^{-k}$*, where* Λ *is the intensity measure.*

Definition 2.7 *Let* Y *be the Poisson point process with an intensity measure* Λ*. For* $F \in \mathfrak{N}$*, denote* $\Pi(F) = P(Y \in F)$*. A point process* X *is* given by a density $f : \mathcal{N} \to \mathbb{R}$ with respect to the Poisson point process Y *if*

$$P(X \in F) = \int_F f(\mathbf{x}) \Pi(d\mathbf{x}).$$

Definition 2.8 *A function* $f : \mathcal{N} \to \mathbb{R}$ *is called* hereditary *if for all finite configurations* $\mathbf{x}, \mathbf{y} \in \mathcal{N}$ *such that* $\mathbf{x} \subset \mathbf{y}$*, it holds that* $f(\mathbf{x}) > 0$ *whenever* $f(\mathbf{y}) > 0$*.*

Definition 2.9 *Let* X *be a point process with an hereditary density* f*. For all finite configurations* $\mathbf{x} \in \mathcal{N}$ *and all points* $v \in \mathbb{R}^d \setminus \mathbf{x}$*, the* Papangelou conditional intensity *is defined as*

$$\begin{aligned} \lambda(\mathbf{x}, v) &= f(\mathbf{x} \cup \{v\}) / f(\mathbf{x}) && \text{if } f(\mathbf{x}) > 0, \\ &= 0 && \text{otherwise.} \end{aligned}$$

Definition 2.10 *Consider a symmetric, reflexive relation* $\sim$ *defined on* $\mathbb{R}^d$ *called* neighborhood*. If two points* $u, v \in \mathbb{R}^d$ *satisfy* $u \sim v$*, they are called* neighbors*.*

Definition 2.11 *A density* $f : \mathcal{N} \to \mathbb{R}^+$ *such that the corresponding Papangelou conditional intensity* $\lambda(\mathbf{x}, v)$ *depends on* $\mathbf{x}$ *only through* $\{u \in \mathbf{x} : u \sim v\}$*, i.e. through the neighbors in* $\mathbf{x}$ *to* v*, is called a* Markov density function*.*

Definition 2.12 *A point process given by a density* $f : \mathcal{N} \to \mathbb{R}^+$ *which is a Markov density function with respect to a neighborhood* $\sim$*, is said to be* Markov *with respect to* $\sim$*.*

Definition 2.13 *A function* $\Phi : \mathcal{N} \to \mathbb{R}^+$ *is called an* interaction function *if* $\Phi(\mathbf{x}) = 1$ *whenever there exist* $u, v \in \mathbf{x}$ *such that* $u \nsim v$*.*

Theorem 2.1 (Hammersley-Clifford) *A hereditary Markov density function $f : \mathcal{N} \to \mathbb{R}^+$ is a density of a Markov point process if and only if there exists an interaction function Φ such that*

$$f(\mathbf{x}) = \prod_{\mathbf{y} \subseteq \mathbf{x}} \Phi(\mathbf{y}), \quad \mathbf{x} \in \mathcal{N}.$$

When speaking about Markov point processes, we suppose that the relation $\sim$ does not depend on the configuration $\mathbf{x}$. However, in the theory of point processes, there was developed a wider class of point processes, so called *nearest neighbor Markov point processes* which are very similar to the Markov processes described above, but with the difference that the relation neighborhood depends on the configuration $\mathbf{x}$, i.e. two points $u, v \in \mathbf{x}_1$ which are neighbors with respect to $\sim$, do not need to be neighbors with respect to the same relation when lying in another configuration $\mathbf{x}_2$. Nevertheless, Baddeley and Møller in [2] show that many relations derived for Markov point processes hold also for the nearest neighbor Markov point processes, including Hammersley-Clifford theorem introduced above.

Definition 2.14 *A density $f : \mathcal{N} \to \mathbb{R}$ is called* Ruelle stable *if there exist positive constants α and β such that $f(\mathbf{x}) \leq \alpha\beta^{n(\mathbf{x})}$ for all $\mathbf{x} \in \mathcal{N}$, where $n(\mathbf{x})$ denotes the number of points in the configuration $\mathbf{x}$.*

Definition 2.15 *A density $f : \mathcal{N} \to \mathbb{R}$ is called* locally stable *if there exists a constant β such that $\lambda(\mathbf{x}, v) \leq \beta$ for all $\mathbf{x} \in \mathcal{N}$ and all $v \in \mathbb{R}^d \setminus \mathbf{x}$.*

Remark 2.1 *It holds that local stability implies Ruelle stability and moreover, both the stability properties imply integrability of the density with respect to Π.*

2.2 Random sets

Definition 2.16 *Let $(\Omega, \mathcal{F}, P)$ be a probability space, $\mathcal{C}$ is a system of all closed sets and $\mathfrak{C} = \sigma\{\mathcal{C}^K : K$ is a compact subset of $\mathbb{R}^d\}$, where $\mathcal{C}^K = \{C \in \mathcal{C} : C \cap K \neq \emptyset\}$. Then a* random closed set $\mathbf{X}$ *in $\mathbb{R}^d$ is a measurable mapping from $(\Omega, \mathcal{F})$ to $(\mathcal{C}, \mathfrak{C})$.*

Definition 2.17 *The* distribution $P_{\mathbf{X}}$ *of a random set $\mathbf{X}$ is given by the relation $P_{\mathbf{X}}(F) = P(\{\omega \in \Omega : \mathbf{X}(\omega) \in F\})$ for $F \in \mathfrak{C}$.*

Definition 2.18 *A random set $\mathbf{X}$ is* stationary *if its distribution is invariant under translation, i.e. for all $v \in \mathbb{R}^d$, the distribution of $\mathbf{X} + v = \{u + v, v \in \mathbf{X}\}$ is the same as*

that of $\mathbf{X}$.
A random set $\mathbf{X}$ *is* isotropic *if its distribution is invariant under rotation.*
If a random set is both stationary and isotropic, it is called motion invariant.

For $A, B \subset \mathbb{R}^d$ denote $A \oplus B := \{x + y : x \in A, y \in B\}$ and $|A|$ the d-dimensional Lebesgue measure of the set A.

Definition 2.19 *Let* $Y = \{y_1, y_2, \ldots\}$ *be a stationary Poisson point process in* $\mathbb{R}^d$ *and* $\{\mathbf{B}_1, \mathbf{B}_2, \ldots\}$ *be a sequence independent identically distributed random compact sets in* $\mathbb{R}^d$ *that are independent on* Y. *Further, let* $\mathbf{B}_0$ *be a random compact set in* $\mathbb{R}^d$ *independent on* $\{\mathbf{B}_1, \mathbf{B}_2, \ldots\}$ *with the same distribution as* $\mathbf{B}_1$. *If* $\mathbb{E}|\mathbf{B}_0 \oplus K| < \infty$ *for all compact sets* K, *then the random set*

$$\mathbf{B} = \cup_{n=1}^{\infty}(y_n + \mathbf{B}_n) \tag{2.2.0.1}$$

is called the Boolean model.

Definition 2.20 *The points* $y_1, y_2, \ldots$ *from Definition 2.19 are called the* germs *and the random sets* $\mathbf{B}_1, \mathbf{B}_2, \ldots$ *are called the* grains *of the Boolean model. The random set* $\mathbf{B}_0$ *is then called the* primary grain.

Definition 2.21 *For a stationary random set* $\mathbf{X}$, *the* volume fraction *(or* area fraction *in the case of* $\mathbb{R}^2$*) is defined by*

$$p = \mathbb{E}|\mathbf{X} \cap C_0|,$$

where C_0 *denotes a unit cube.*

Proposition 2.2 *For a stationary Boolean model (2.2.0.1) with intensity of germs* ρ, *the volume fraction is given by*

$$p = 1 - \exp(-\rho\mathbb{E}|\mathbf{B}_0|).$$

Definition 2.22 *For a stationary random set* $\mathbf{X}$ *and a convex compact set* $K \subset \mathbb{R}^d$ *containing the origin, let*

$$D = \inf\{r \geq 0 : \mathbf{X} \cap rK \neq \emptyset\}$$

where $rK = \{(rx, ry) : (x, y) \in K\}$. *Assuming* $\mathrm{P}(D > 0) > 0$, *the* contact distribution function *with structuring element* K *is defined by*

$$H_K(r) = \mathrm{P}(D \leq r | D > 0), \quad r \geq 0.$$

Proposition 2.3 *For a stationary Boolean model (2.2.0.1) with intensity of germs ρ, the contact distribution function is given by*

$$H_K(r) = 1 - \exp(-\rho(\mathbb{E}|\mathbf{B}_0 + rK| - \mathbb{E}|\mathbf{B}_0|)), \quad r \geq 0.$$

Definition 2.23 *For a stationary random set $\mathbf{X}$, the* covariance function *is defined by*

$$C(v) = P(o \in \mathbf{X}, v \in \mathbf{X}), \quad v \in \mathbb{R}^d,$$

where o denotes the origin.

Proposition 2.4 *For a stationary Boolean model (2.2.0.1) with intensity of germs ρ, the covariance function is given by*

$$C(v) = 2p - 1 + (1-p)^2 \exp(\rho\mathbb{E}|\mathbf{B}_0 \cap (\mathbf{B}_0 - v)|).$$

Remark 2.2 *For a motion invariant random set $\mathbf{X}$, the covariance function is defined as a function of a real variable*

$$C(r) = C(re), \quad r \in \mathbb{R},$$

where e is some unit vector in $\mathbb{R}^d$, i.e. the definition is equivalent to the relation

$$C(r) = \mathrm{P}(u \in \mathbf{X},\, v \in \mathbf{X})$$

for any two points $u, v \in \mathbb{R}^d$ with distance $\|u-v\| = r$, where $\|\cdot\|$ denotes usual Euclidean distance.

Chapter 3

Random union of interacting discs

3.1 Basic notation and setup

3.1.1 Model density

By a disc with center $z \in \mathbb{R}^2$ and positive radius $r > 0$ we mean a two-dimensional closed set $b = \{y \in \mathbb{R}^2 : \|y - z\| \leq r\}$. We identify b with the point $x = (z, r)$ in $\mathbb{R}^2 \times (0, \infty)$, and write $b = b(x) = b(z, r)$. Similarly, we identify the processes of discs $b_i = b(z_i, r_i)$ with point processes on $\mathbb{R}^2 \times (0, \infty)$.

The reference process will be a process $\mathbf{Y}$ of discs corresponding to a Poisson point process Y on $\mathbb{R}^2 \times (0, \infty)$ with an intensity measure of the form $\rho(z)\,\mathrm{d}z\,Q(\mathrm{d}r)$, where $\mathrm{d}z$ is Lebesgue measure on $\mathbb{R}^2$ and Q is an arbitrary probability measure on $(0, \infty)$ (thus the random set given by the union of discs in $\mathbf{Y}$ is a Boolean model).

Furthermore, local integrability of ρ is assumed to ensure that with probability one, the point process of the centers of the discs in S is finite for any bounded region $S \subset \mathbb{R}^2$. In the sequel, S denotes a given bounded planar region such that $\int_S \rho(z)\,\mathrm{d}z > 0$.

The object of primary interest is the random closed set $\mathcal{U}_X = \cup_{x \in X} b(x)$ where X is a finite point process defined on $S \times (0, \infty)$, and as mentioned above, we will sometimes exchange the point process X with the corresponding disc process $\mathbf{X}$. If $\mathbf{X} = \emptyset$ is the empty configuration, we let $\mathcal{U}_{\mathbf{X}} = \mathcal{U}_X = \emptyset$ be the empty set. Note that the centers of the discs are contained in S but the discs may extend outside S.

We assume that $\mathbf{X}$ is absolutely continuous with respect to the reference process $\mathbf{Y}$ and given by a density $f(\mathbf{x})$ with respect to $\mathbf{Y}$ for finite configurations $\mathbf{x} = \{x_1, \ldots, x_n\}$ with

$x_i = (z_i, r_i) \in S \times (0, \infty)$ and $0 \leq n < \infty$ (if $n = 0$ then $\mathbf{x}$ is the empty configuration).

We focus on the case where the density is of the exponential family form

$$f_\theta(\mathbf{x}) = \exp\left(\theta \cdot T(\mathcal{U}_\mathbf{x})\right) / c_\theta \tag{3.1.1.1}$$

where θ is a real parameter vector, $\cdot$ denotes the usual inner product, $T(\mathcal{U}_\mathbf{x})$ is a statistic of the same dimension as θ, and c_θ is a normalizing constant depending on θ (and of course also on (T, ρ, Q)).

Remark 3.1 *In fact, (3.1.1.1) is the density of a disc process with respect to the Boolean model with the intensity of germs $\rho = 1$. When having the Boolean model with a general intensity function of germs $\rho(z)$ as a reference process, it has to be multiplied by the term $\prod_{i=1}^{n(\mathbf{x})} \rho(z_i)$, where $n(\mathbf{x})$ denotes the number of discs in the configuration $\mathbf{x}$. However, it is not significant for deriving the theoretical results and it is obvious how to work with the general form of the density when simulating the process and when deriving the statistical inference, therefore we will for simplicity omit this term in the whole work.*

Remark 3.2 *Note also that the normalizing constant*

$$\begin{aligned} c_\theta = &\exp\left(-\int_S \rho(z)\,\mathrm{d}z\right) \times \left[\exp(\theta \cdot T(\emptyset)) + \sum_{n=1}^{\infty} \frac{1}{n!} \int_S \int_0^\infty \cdots \int_S \int_0^\infty \right. \\ &\left. \exp\left(\theta \cdot T\left(\mathcal{U}_{\{(z_1,r_1),\ldots,(z_n,r_n)\}}\right)\right) \prod_1^n \rho(z_i)\,\mathrm{d}z_1\, Q(\mathrm{d}r_1) \cdots \mathrm{d}z_n\, Q(\mathrm{d}r_n)\right] \end{aligned} \tag{3.1.1.2}$$

is in general not expressible in closed form unless $\theta \neq 0$ (which correspond to the reference Boolean model).

3.1.2 General position of discs

Definition 3.1 *For a disc $b(z, r)$, define the* ghost sphere *as $s(z, r) = \{y \in \mathbb{R}^3 : \|y - z\| = r\}$, i.e. the hypersphere in $\mathbb{R}^3$ with center z and radius r.*

Definition 3.2 *A configuration of discs is said to be in* general position *if the intersection of any $k + 1$ corresponding ghost spheres is either empty or a sphere of dimension $2 - k$, where $k = 1, 2, \ldots$*

Note that the intersection is assumed to be empty if $k > 2$, and a sphere of dimension 0 is assumed to consists of two points. The left panel in Figure 3.1 shows a configuration of discs in general position.

Remark 3.3 *In fact, being in general position means that the nonempty intersection of two discs is a 2-dimensional set and not exactly one point.*

Lemma 3.1 *For almost all realizations of* $\mathbf{Y} = \{y_1, y_2, \ldots\}$*, the discs* $b_1 = b(y_1),\ b_2 = b(y_2),\ \ldots$ *are in general position.*

Proof. See [14].

□

It follows from Lemma 3.1 and the assumption on $\mathbf{X}$ that the discs in $\mathbf{X}$ with density (3.1.1.1) are in general position almost surely. Therefore we will assume this condition for the rest of the work and we will not introduce it any more.

3.2 Power tessellation of a union of discs

This section defines and studies the power tessellation of a union of discs $\mathcal{U} = \cup_{i \in I} b_i$ (in general, I does not need to be finite) which is very useful tool for deriving some of the theoretical results introduced in Section 3.3 and mainly for simulation described in Section 3.4.

We assume that the discs b_i satisfy the general position assumption (henceforth GPA).

3.2.1 Basic definitions

For each disc b_i $(i \in I)$ with ghost sphere s_i, let $s_i^+ = \{(y_1, y_2, y_3) \in s_i : y_3 \geq 0\}$ denote the corresponding upper hypersphere, and for $u \in b_i$, let $y_i(u)$ denote the unique point on s_i^+ such that its orthogonal projection on $\mathbb{R}^2$ is u. The subset of s_i^+ consisting of those points "we can see from above" is given by

$$C_i = \{y_i(u) : u \in b_i,\ \|u - y_i(u)\| \geq \|u - y_j(u)\| \text{ whenever } u \in b_j,\ j \in I\},$$

and the GPA implies that the non-empty C_i have disjoint 2-dimensional relative interiors. Further, let B_i denote the orthogonal projection of C_i on $\mathbb{R}^2$ and $J = \{i \in I : C_i \neq \emptyset\}$.

Definition 3.3 *The collection* $\mathcal{B}$ *of sets* $B_i,\ i \in J$ *is called the* power tessellation *of the union of discs.*

An example of such a tessellation is shown in the lower left panel in Figure 3.1. Note that the collection of B_i constitutes a subdivision of $\mathcal{U}$ into 2-dimensional convex sets with disjoint interiors. This fact becomes very useful when calculating values of geometrical characteristics of the union.

An other point of view to the power tessellation is through Laguerre diagrams.

Definition 3.4 *For $i \in I$, define the* power distance *of a point $u \in \mathbb{R}^2$ from $b_i = b(z_i, r_i)$ by $\pi_i(u) = \|u - z_i\|^2 - r_i^2$, and consequently the* power cell *associated with b_i by*

$$V_i = \{u \in \mathbb{R}^2 : \pi_i(u) \leq \pi_j(u) \text{ for all } j \in I\}.$$

For $i, j \in I$, define the closed half-plane $H_{i,j} = \{u \in \mathbb{R}^2 : \pi_i(u) \leq \pi_j(u)\}$. Each V_i is a convex polygon, since it is a finite intersection of closed half-planes $H_{i,j}$. The power cells have disjoint interiors, and by GPA, each V_i is either empty or two dimensional set.

Definition 3.5 *A tessellation consisted of the non-empty power cells V_i, $i \in J$ is called the* power diagram *(or* Laguerre diagram*).*

Remark 3.4 *In the special case where all radii r_i are equal, we have $I = J$ and the power diagram is a Voronoi tessellation (see e.g. [19]) where each cell V_i contains z_i in its interior. However, if the radii are not equal, a power cell V_i may not contain z_i, since $H_{i,j}$ may not contain z_i as seen in Figure 3.1.*

By Pythagoras, for all $u \in b_i$ it holds that $\pi_i(u) + \|u - y_i(u)\|^2 = 0$ and consequently, for any $i, j \in I$ and $u \in b_i \cap b_j$,

$$\|u - y_i(u)\| \geq \|u - y_j(u)\| \quad \text{if and only if} \quad \pi_i(u) \leq \pi_j(u).$$

Thus the cells of the power tessellation are given by $B_i = V_i \cap b_i$.

Further in the work, we will use terms introduced in the following definitions.

Definition 3.6 *We say that a cell B_i is an* isolated cell *if $B_i = b_i$.*

Remark 3.5 *Note that the definition means that any disc b_j, $j \in I$, intersecting b_i is whole contained in b_i.*

Definition 3.7 *If the intersection $e_{i,j} = B_i \cap B_j$ between two cells of $\mathcal{B}$ is non-empty, then the closed line segment $e_{i,j} = [u_{i,j}, v_{i,j}]$, where $u_{i,j}$ and $v_{i,j}$ denote the endpoints, is called an* interior edge *of $\mathcal{B}$.*

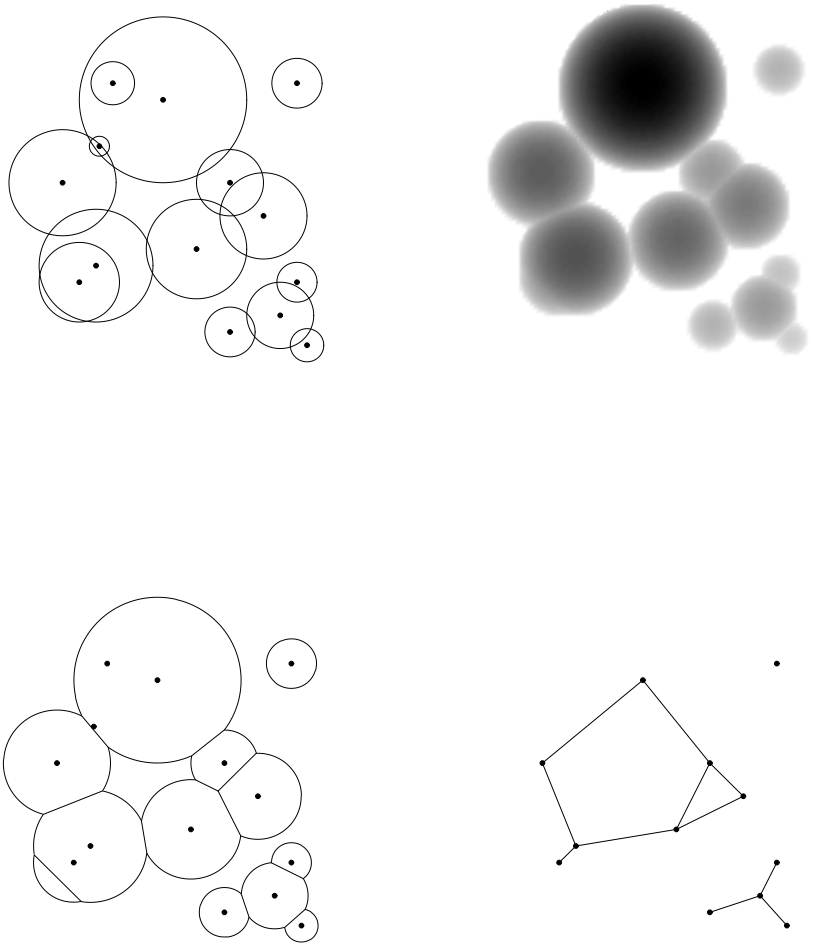

Figure 3.1: Upper left panel: A configuration of discs in general position. Upper right panel: The upper hemispheres as seen from above. Lower left panel: The power tessellation of the union of discs. Lower right panel: The dual graph.

Definition 3.8 *The* vertices *of $\mathcal{B}$ are given by all endpoints of interior edges. A vertex of $\mathcal{B}$ lying on the boundary $\partial\mathcal{U}$ is called a* boundary vertex*, and it is called an* interior vertex *otherwise.*

Definition 3.9 *Each circular arc on $\mathcal{B}$ bounded by two successive boundary vertices is called a* boundary edge *of $\mathcal{B}$. The circle given by the boundary of an isolated cell of $\mathcal{B}$ is also called a boundary edge or sometimes an* isolated boundary edge*. A boundary edge of $\mathcal{B}$ is written as $\lfloor u_i, v_i \rceil$ if $B_i \neq b_i$ (a non-isolated cell), where the index means that u_i and v_i are boundary vertices of B_i ordered anti-clockwise, or as ∂b_i if $B_i = b_i$.*

By GPA, any intersection among four cells of $\mathcal{B}$ is empty, each interior vertex corresponds to a non-empty intersection among three cells of $\mathcal{B}$, and exactly three edges emerge at each vertex. Each interior edge $e_{i,j}$ is contained in the bisector of b_i and b_j defined by $\partial H_{i,j} = \{u \in \mathbb{R}^d : \pi_i(u) = \pi_j(u)\}$. This is the line perpendicular to the line joining the centers of the two discs, and passing through the point

$$z_{i,j} = \frac{1}{2}\left(z_i + z_j + \frac{r_j^2 - r_i^2}{\|z_i - z_j\|^2}(z_i - z_j)\right).$$

Definition 3.10 *We call $E_{i,j} \equiv \partial H_{i,j} \cap b_i = \partial H_{i,j} \cap b_j$ the* chord *of $b_i \cap b_j$. Obviously, $e_{i,j} \subseteq E_{i,j}$.*

Definition 3.11 *The* dual graph *$\mathcal{D}$ to $\mathcal{B}$ has nodes equal to the centers z_i, $i \in J$ of discs generating non-empty cells, and each edge of $\mathcal{D}$ is given by two vertices z_i and z_j such that $e_{i,j} \neq \emptyset$.*

For an example of a dual graph, see the lower right panel in Figure 3.1. Note that there is a one-to-one correspondence between the edges of $\mathcal{D}$ and the interior edges of $\mathcal{B}$.

3.2.2 Construction

We can construct the power tessellation of a finite union of discs by adding the discs one by one, keeping track on old and new edges and whether each disc generates a non-empty cell or not. This becomes very useful in software solution of the "birth-part" of the MCMC algorithm (described in Section 3.4), because it makes the computation local in the sense that only the cells of the tessellation which are intersected by a newly added disc are changed.

Moreover, we describe in this section, how to construct the tessellation in the case when an old ball is deleted from the given union, assuming that the old power tessellation is known. This is then used in software solution of the "death-part" of the MCMC algorithm.

I. The case when a new disc is added

Suppose we want to construct a new power tessellation $\mathcal{B}^{\text{new}}$ of a union $\mathcal{U}^{\text{new}} = \cup_1^n b_i$ of $n \geq 1$ discs in general position, where we are adding the disc b_n and we have already constructed the power tessellation $\mathcal{B}^{\text{old}}$ of $\mathcal{U}^{\text{old}} = \cup_1^{n-1} b_i$ based on the $n-1$ other discs (if $n = 1$ then $\mathcal{B}^{\text{old}}$ and $\mathcal{U}^{\text{old}}$ are empty). More precisely, with respect to $\mathcal{B}^{\text{old}}$, we assume to know all the old edges. We denote old interior edges by $[u_{i,j}^{\text{old}}, v_{i,j}^{\text{old}}]$ and old boundary edges by $\lfloor u_i^{\text{old}}, v_i^{\text{old}} \rceil$ or $\partial b_i^{\text{old}}$. We want to construct the new tessellation $\mathcal{B}^{\text{new}}$ of $\mathcal{U}^{\text{new}} = \mathcal{U}^{\text{old}} \cup b_n$ by finding its interior edges $[u_{i,n}^{\text{new}}, v_{i,n}^{\text{new}}]$ and boundary edges $\lfloor u_n^{\text{new}}, v_n^{\text{new}} \rceil$ associated to the new cell B_n^{new}. This is done in steps (ii) and (iv) below. Moreover, to obtain the remaining new edges, we modify old interior edges $[u_{i,j}^{\text{old}}, v_{i,j}^{\text{old}}]$ and old boundary edges $\lfloor u_i^{\text{old}}, v_i^{\text{old}} \rceil$ or $\partial b_i^{\text{old}}$, noticing that a "modified old edge" can be unchanged, reduced or disappearing. This is done in steps (iii) and (v) below. Notice that steps (i), (ii), and (iv) determine the new cells, i.e. which of the sets $B_1^{\text{new}}, \ldots, B_n^{\text{new}}$ are empty or not.

(i) Considering old discs intersecting the new disc: If b_n is contained in some disc b_j with $j < n$, then B_n^{new} is empty and so $\mathcal{B}^{\text{new}} = \mathcal{B}^{\text{old}}$ is unchanged. Assume that b_n is not contained in any disc b_j with $j < n$, and without loss of generality that b_n intersects $B_1^{\text{old}}, \ldots, B_i^{\text{old}}$ but not $B_{i+1}^{\text{old}}, \ldots, B_{n-1}^{\text{old}}$, where $0 \leq i \leq n-1$ (setting $i = 0$ if b_n has no intersection). Then $B_j^{\text{new}} = B_j^{\text{old}}$ is unchanged for $j = i+1, \ldots, n-1$, so it suffices below to find the edges of $B_1^{\text{new}}, \ldots, B_i^{\text{new}}$ and B_n^{new}, when in the case $i = 0$, the only change is that $B_n^{\text{new}} = b_n$ is an isolated cell with boundary edge ∂b_n.

In (ii)-(vi) we assume that $i \geq 1$.

(ii) Finding the interior edges of B_n^{new}: To obtain the interior edges of B_n^{new}, for $j = 1, \ldots, i$, we start by assigning $e_{j,n}^{\text{new}} \leftarrow [u_{j,n}^{\text{new}}, v_{j,n}^{\text{new}}]$, considering $u_{j,n}^{\text{new}}$ and $v_{j,n}^{\text{new}}$ as (potential) boundary vertices given by the endpoints of the chord $E_{j,n}$. Further, for $k = 1, \ldots, i$ with $k \neq j$, if $e_{j,n}^{\text{new}} \cap H_{n,k} = \emptyset$ (or equivalently $u_{j,n}^{\text{new}} \notin H_{n,k}$ and $v_{j,n}^{\text{new}} \notin H_{n,k}$, since $H_{n,k}$ is convex) we obtain that $e_{j,n}^{\text{new}} \leftarrow \emptyset$ and we can stop the k-loop, else $e_{j,n}^{\text{new}} \leftarrow e_{j,n}^{\text{new}} \cap H_{n,k}$. In the latter case, either both vertices are contained in $H_{n,k}$ and so the edge remains unchanged, or exactly one vertex is not contained in $H_{n,k}$, e.g. $u_{j,n}^{\text{new}} \notin H_{n,k}$ but $v_{j,n}^{\text{new}} \in H_{n,k}$, in which case $u_{j,n}^{\text{new}}$ becomes an interior vertex given by the point $e_{j,n}^{\text{new}} \cap \partial H_{n,k}$ while $v_{j,n}^{\text{new}}$ is unchanged. In this way we find all interior edges of B_n^{new}, and all interior and boundary vertices of B_n^{new}.

Since we have assumed that $i > 0$, B_n^{new} is empty if and only if it has no interior edges.

(iii) Modifying the old interior edges: At the same time as we do step (ii) above, we also check whether each interior edge $e^{\text{old}}_{j,k} = [u^{\text{old}}_{j,k}, v^{\text{old}}_{j,k}]$ of $\mathcal{B}^{\text{old}}$ with $j < k \leq i$ should be kept, reduced or omitted when we consider $\mathcal{B}^{\text{new}}$ (recalling that $e^{\text{new}}_{j,k} = e^{\text{old}}_{j,k}$ is unchanged if $j > i$ or $k > i$). We have

$$e^{\text{new}}_{j,k} = e^{\text{old}}_{j,k} \cap H_{j,n} = e^{\text{old}}_{j,k} \cap H_{k,n}.$$

Thus $e^{\text{new}}_{j,k}$ is empty if $u^{\text{old}}_{j,k} \notin H_{k,n}$ and $v^{\text{old}}_{j,k} \notin H_{k,n}$, while $e^{\text{new}}_{j,k} = e^{\text{old}}_{j,k}$ if $u^{\text{old}}_{j,k} \in H_{k,n}$ and $v^{\text{old}}_{j,k} \in H_{k,n}$. Further, if $u^{\text{old}}_{j,k} \in H_{k,n}$ and $v^{\text{old}}_{j,k} \notin H_{k,n}$, then $e^{\text{new}}_{j,k} = [u^{\text{old}}_{j,k}, v^{\text{new}}_{j,k}]$ where $v^{\text{new}}_{j,k}$ is the point given by $e^{\text{old}}_{j,k} \cap \partial H_{k,n}$. Similarly, if $u^{\text{old}}_{j,k} \notin H_{k,n}$ and $v^{\text{old}}_{j,k} \in H_{k,n}$, then $e^{\text{new}}_{j,k} = [u^{\text{new}}_{j,k}, v^{\text{old}}_{j,k}]$ where $u^{\text{new}}_{j,k}$ is the point given by $e^{\text{old}}_{j,k} \cap \partial H_{k,n}$.

Note that for each $j \leq i$, B^{new}_j is empty if and only if it has no interior edge.

(iv) Finding the boundary edges of B^{new}_n: Suppose that B^{new}_n has $m > 0$ boundary vertices $w^{\text{new}}_1, \dots, w^{\text{new}}_m$. Notice that m is an even number, and we can organize the boundary vertices such that $w^{\text{new}}_1 = z_n + r_n(\cos\varphi^{\text{new}}_1, \sin\varphi^{\text{new}}_1)$, …, $w^{\text{new}}_m = z_n + r_n(\cos\varphi^{\text{new}}_m, \sin\varphi^{\text{new}}_m)$, where $0 \leq \varphi^{\text{new}}_1 < \cdots < \varphi^{\text{new}}_m < 2\pi$. Then B^{new}_n has $m/2$ boundary edges, namely

$$\lfloor w^{\text{new}}_2, w^{\text{new}}_3 \rceil, \lfloor w^{\text{new}}_4, w^{\text{new}}_5 \rceil, \dots, \lfloor w^{\text{new}}_m, w^{\text{new}}_1 \rceil \quad \text{if } z_n + (r_n, 0) \in H_{n,j} \text{ for all } j = 1, \dots, i$$

and

$$\lfloor w^{\text{new}}_1, w^{\text{new}}_2 \rceil, \lfloor w^{\text{new}}_3, w^{\text{new}}_4 \rceil, \dots, \lfloor w^{\text{new}}_{m-1}, w^{\text{new}}_m \rceil \quad \text{otherwise.}$$

(v) Modifying the old boundary edges: Finally, we modify the boundary edges $\lfloor u^{\text{old}}_j, v^{\text{old}}_j \rceil$ of $\mathcal{B}^{\text{old}}$ considering $\mathcal{B}^{\text{new}}$ and $j \leq i$ (noticing that $\lfloor u^{\text{old}}_j, v^{\text{old}}_j \rceil$ is a boundary edge of $\mathcal{B}^{\text{new}}$ too if $j > i$). This is done in a similar way as in step (iv). Suppose that B^{new}_j has $m_j > 0$ boundary vertices $w^{\text{new}}_1, \dots, w^{\text{new}}_{m_j}$, which we organize as in (iv). Then B^{new}_j has boundary edges

$$\lfloor w^{\text{new}}_2, w^{\text{new}}_3 \rceil, \lfloor w^{\text{new}}_4, w^{\text{new}}_5 \rceil, \dots, \lfloor w^{\text{new}}_{m_j}, w^{\text{new}}_1 \rceil$$
$$\text{if } z_j + (r_j, 0) \in H_{j,k} \text{ for all } k \leq n \text{ with } k \neq j \text{ and } b_j \cap b_k \neq \emptyset$$

and

$$\lfloor w^{\text{new}}_1, w^{\text{new}}_2 \rceil, \lfloor w^{\text{new}}_3, w^{\text{new}}_4 \rceil, \dots, \lfloor w^{\text{new}}_{m_{j-1}}, w^{\text{new}}_{m_j} \rceil \quad \text{otherwise.}$$

II. The case when a disc is deleted

Suppose we are deleting the disc b_n from a configuration $\{b_1, \dots, b_n\}$ of $n \geq 1$ discs, which are assumed to be in general position. We also assume that we know the power tessellation $\mathcal{B}^{\text{old}}$ of $\mathcal{U}^{\text{old}} = \cup_1^n b_i$. Below we explain how to construct the new power tessellation $\mathcal{B}^{\text{new}}$ of $\mathcal{U}^{\text{new}} = \cup_1^{n-1} b_i$. More precisely, with respect to $\mathcal{B}^{\text{old}}$, we assume to know all the

interior edges $[u_{i,j}^{\text{old}}, v_{i,j}^{\text{old}}]$ and all the boundary edges $\lfloor u_i^{\text{old}}, v_i^{\text{old}} \rceil$. We want to construct the tessellation $\mathcal{B}^{\text{new}}$ of $\mathcal{U}^{\text{new}} = \mathcal{U}^{\text{old}} \setminus b_n$ by finding the interior edges $[u_{i,j}^{\text{new}}, v_{i,j}^{\text{new}}]$ and the boundary edges $\lfloor u_i^{\text{new}}, v_i^{\text{new}} \rceil$ associated to each new cell B_i^{new}, noticing that B_i^{new} either agrees with B_i^{old} or is an enlargement of B_i^{old} or is a completely new cell. One possibility could be to "reverse" the construction in I., where a new disc is added, however, we realized that it is easier to create the new edges without reversing the construction in I. but using a construction as described below. This is partly explained by the fact that an old empty set B_i^{old} may possibly be replaced by a non-empty set B_i^{new}.

(i) Considering the discs intersecting the disc which is deleted: Clearly, if B_n^{old} is empty, then $\mathcal{B}^{\text{new}} = \mathcal{B}^{\text{old}}$ is unchanged. Assume that B_n^{old} is a non-empty cell, and without loss of generality that b_n intersects $b_1, \dots, b_i$ but not $b_{i+1}, \dots, b_{n-1}$, where $0 \leq i \leq n-1$ (setting $i = 0$ if b_n has no intersection). Then it suffices to find the edges of $B_1^{\text{new}}, \dots, B_i^{\text{new}}$, since $B_j^{\text{new}} = B_j^{\text{old}}$ is unchanged for $j = i+1, \dots, n-1$. If $i = 0$ then $B_n^{\text{old}} = b_n$ is an isolated cell, and so $B_1^{\text{new}} = B_1^{\text{old}}, \dots, B_{n-1}^{\text{new}} = B_{n-1}^{\text{old}}$ are unchanged. In the following steps (ii)-(iv), suppose that $i > 0$.

(ii) Finding the new interior edges: If $i = 1$, no new interior edge appears. Suppose that $i \geq 2$. We want to determine each set $e_{j,k}^{\text{new}}$ with $j < k \leq i$. We start by assigning all cells $B_1^{\text{new}}, \dots, B_i^{\text{new}}$ to be non-empty, and by assigning $e_{j,k}^{\text{new}} \leftarrow [u_{j,k}^{\text{new}}, v_{j,k}^{\text{new}}]$, considering $u_{j,k}^{\text{new}}$ and $v_{j,k}^{\text{new}}$ as (potential) boundary vertices given by the endpoints of the chord $E_{j,k}$. Consider a loop with $l = 1, \dots, i$ and $l \neq j, k$. If $e_{j,k}^{\text{new}} \cap H_{k,l} = \emptyset$ (or equivalently $u_{j,k}^{\text{new}} \notin H_{k,l}$ and $v_{j,k}^{\text{new}} \notin H_{k,l}$, since $H_{k,l}$ is convex), we have that $e_{j,k}^{\text{new}}$ is empty and we can stop the l-loop. Otherwise assign $e_{j,k}^{\text{new}} \leftarrow e_{j,k}^{\text{new}} \cap H_{k,l}$, where we notice that only the following two cases can occur. First, if both vertices of $e_{j,k}^{\text{new}}$ are contained in $H_{k,l}$, the edge remains unchanged. Secondly, if exactly one vertex is not contained in $H_{k,l}$, e.g. $u_{j,k}^{\text{new}} \notin H_{k,l}$ but $v_{j,k}^{\text{new}} \in H_{k,l}$, then $u_{j,k}^{\text{new}}$ becomes an interior vertex given by the point $e_{j,k}^{\text{new}} \cap \partial H_{k,l}$ while $v_{j,k}^{\text{new}}$ is unchanged. When the loop is finished, we have determined all the new interior edges, including the information whether their endpoints are interior or boundary vertices.

(iii) Determining the new cells: For each $j \leq i$, we determine if B_j^{new} is a new cell by checking if it has an edge. Suppose that B_j^{new} has no interior edge, i.e. it is either an empty set or a new isolated cell. If an arbitrary fixed point of b_j is included in $H_{j,l}$ for all $l = 1, \dots, n-1$ with $l \neq j$, then B_j has exactly one boundary edge and it is an isolated cell. Otherwise B_j^{new} is empty. In this way we determine whether each B_j^{new} is empty or a new cell, including whether it is an isolated cell.

(iv) Finding the new boundary edges: We have already determined the new isolated boundary edges in step (iii). Consider a non-isolated cell B_j^{new} with $j \leq i$ with boundary vertices $w_k^{\text{new}} = z_j + r_j(\cos\varphi_k^{\text{new}}, \sin\varphi_k^{\text{new}})$, $k = 1, \dots, m_j$. Recall that $m_j > 0$ is an even number and we organize the vertices so that $0 \leq \varphi_1^{\text{new}} < \dots < \varphi_{m_j}^{\text{new}} < 2\pi$, cf. (iv) in I.

Then B_j^{new} has $m_j/2$ boundary edges, namely

$$\lfloor w_2^{\text{new}}, w_3^{\text{new}} \rceil, \lfloor w_4^{\text{new}}, w_5^{\text{new}} \rceil, \ldots, \lfloor w_{m_j}^{\text{new}}, w_1^{\text{new}} \rceil \quad \text{if } z_j + (r_j, 0) \in H_{j,l} \text{ for all } l = 1, \ldots, i$$

and

$$\lfloor w_1^{\text{new}}, w_2^{\text{new}} \rceil, \lfloor w_3^{\text{new}}, w_4^{\text{new}} \rceil, \ldots, \lfloor w_{m_j-1}^{\text{new}}, w_{m_j}^{\text{new}} \rceil \quad \text{otherwise.}$$

3.3 Theoretical results

This section studies the disc process $\mathbf{X}$ as specified by the density $f(\mathbf{x})$ in (3.1.1.1).

3.3.1 Specification of the density

We will denote $\mathcal{U}_{\mathbf{x}}$ the union of discs corresponding to the configuration $\mathbf{x} = \{x_1, \ldots, x_n\}$ and assume that the statistic $T(\mathcal{U}_{\mathbf{x}})$ is a linear combination of one or more of the following geometric characteristics:

- the area $A = A(\mathcal{U}_{\mathbf{x}})$,
- the perimeter $L = L(\mathcal{U}_{\mathbf{x}})$,
- the Euler-Poincaré characteristic $\chi = \chi(\mathcal{U}_{\mathbf{x}})$,
- the number of isolated cells $N_{\text{ic}} = N_{\text{ic}}(\mathcal{U}_{\mathbf{x}})$,
- the number of connected components $N_{\text{cc}} = N_{\text{cc}}(\mathcal{U}_{\mathbf{x}})$,
- the number of holes $N_{\text{h}} = N_{\text{h}}(\mathcal{U}_{\mathbf{x}})$,
- the number of boundary edges (including isolated boundary edges) $N_{\text{be}} = N_{\text{be}}(\mathcal{U}_{\mathbf{x}})$,
- the number of boundary vertices $N_{\text{bv}} = N_{\text{bv}}(\mathcal{U}_{\mathbf{x}})$.

In the general case,

$$T = (A, L, \chi, N_{\text{h}}, N_{\text{ic}}, N_{\text{bv}}) \tag{3.3.1.1}$$

with corresponding parameter $\theta = (\theta_1, \ldots, \theta_6)$, and so the density is in the form

$$f_\theta(\mathbf{x}) = \frac{1}{c_\theta} \exp\left(\theta_1 A(\mathcal{U}_{\mathbf{x}}) + \theta_2 L(\mathcal{U}_{\mathbf{x}}) + \theta_3 \chi(\mathcal{U}_{\mathbf{x}}) + \theta_4 N_{\text{h}}(\mathcal{U}_{\mathbf{x}}) + \theta_5 N_{\text{ic}}(\mathcal{U}_{\mathbf{x}}) + \theta_6 N_{\text{bv}}(\mathcal{U}_{\mathbf{x}})\right). \tag{3.3.1.2}$$

Remark 3.6 *Since the interaction in the model depends on the vector T of geometrical characteristics, we call then* $\mathbf{X}$ *the* T-interaction process. *If e.g.* $\theta_2 = \ldots = \theta_6 = 0$, *we set* $T = A$ *and refer then to the* A-interaction process. *Similarly, for the* L-interaction process *we have* $\theta_1 = 0$ *and* $\theta_3 = \ldots = \theta_6 = 0$, *for the* (A, L)-interaction process *we have* $\theta_3 = \ldots = \theta_6 = 0$, *and so on. A* quermass-interaction process *is the special case* $T = (A, L, \chi)$ *and* $\theta_4 = \theta_5 = \theta_6 = 0$. *In this work, we will often consider the so-called additive extension of the Euler-Poincaré characteristic, i.e.* $\chi = N_{\mathrm{cc}} - N_{\mathrm{h}}$, *thus a* continuum random cluster model *($T = N_{\mathrm{cc}}$) is given by* $\theta_1 = \theta_2 = \theta_5 = \theta_6 = 0$, *and* $\theta_3 = \theta_4$.

3.3.2 Interpretation of parameters

This section discusses the meaning of the parameters $\theta_1, \ldots, \theta_6$ in the T-interaction process. Their meaning is well seen from Papangelou conditional intensity. For all characteristics $G = A, L, \ldots$, define $G(\mathbf{x}, v) = G(\mathcal{U}_{\mathbf{x}\cup\{v\}}) - G(\mathcal{U}_{\mathbf{x}})$ and denote $\mathcal{N}^f$ the set of all finite subsets $\mathbf{x}$ such that the discs $\mathbf{x}$ are in general position. Then the T-interaction process has an hereditary density with Papangelou conditional intensity

$$\lambda_\theta(\mathbf{x}, v) = \exp\left(\theta_1 A(\mathbf{x}, v) + \theta_2 L(\mathbf{x}, v) + \theta_3 \chi(\mathbf{x}, v) + \theta_4 N_{\mathrm{h}}(\mathbf{x}, v) + \theta_5 N_{\mathrm{ic}}(\mathbf{x}, v) + \theta_6 N_{\mathrm{bv}}(\mathbf{x}, v)\right) \tag{3.3.2.1}$$

if $\mathbf{x} \cup \{v\} \in \mathcal{N}^f$, and $\lambda_\theta(\mathbf{x}, v) = 0$ otherwise.

Definition 3.12 *The process* $\mathbf{X}$ *is said to be* attractive *if*

$$\lambda_\theta(\mathbf{x}, v) \geq \lambda_\theta(\mathbf{y}, v) \quad \textit{whenever } \mathbf{y} \subset \mathbf{x},\ \mathbf{x} \in \mathcal{N}^f, \tag{3.3.2.2}$$

and repulsive *if*

$$\lambda_\theta(\mathbf{x}, v) \leq \lambda_\theta(\mathbf{y}, v) \quad \textit{whenever } \mathbf{y} \subset \mathbf{x},\ \mathbf{x} \in \mathcal{N}^f. \tag{3.3.2.3}$$

Note that since quermass integrals are additive,

$$A(\mathbf{x}, v) = A(b_v) - A(b_v \cap \mathcal{U}_{\mathbf{x}}), \quad L(\mathbf{x}, v) = L(b_v) - L(b_v \cap \mathcal{U}_{\mathbf{x}}), \quad \chi(\mathbf{x}, v) = 1 - \chi(b_v \cap \mathcal{U}_{\mathbf{x}}). \tag{3.3.2.4}$$

Proposition 3.2 *We have that*

(a) the A-interaction process is attractive if $\theta_1 < 0$ *and repulsive if* $\theta_1 > 0$;

(b) the G-interaction processes with $G = L, \chi, N_{\mathrm{h}}, N_{\mathrm{ic}}, N_{\mathrm{bv}}$ *are neither attractive nor repulsive if* $\theta_i \neq 0$, $i = 2, \ldots, 6$;

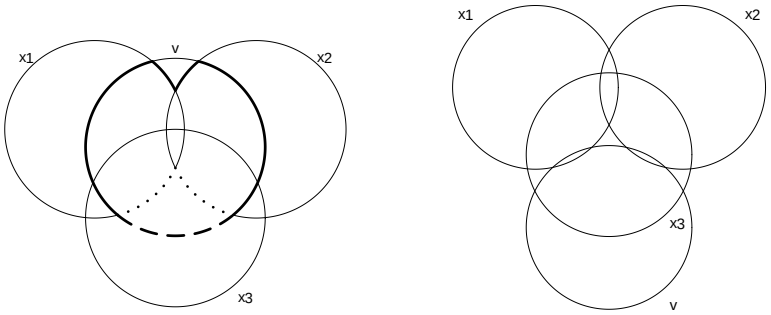

Figure 3.2: Examples of four discs of equal radii. Left panel: When we add x_3 to $\{x_1, x_2\}$ the dotted arcs disappear and the dashed arc appears, so $L(b_v \cap \mathcal{U}_{\{x_1,x_2,x_3\}}) < L(b_v \cap \mathcal{U}_{\{x_1,x_2\}})$. Right panel: $N_{\mathrm{bv}}(\{x_1, x_2\}, v) = 4$ and $N_{\mathrm{bv}}(\{x_1, x_2, x_3\}, v) = 2$.

(c) the continuum random cluster model (i.e. the N_{cc}-interaction process, where $\theta_3 = \theta_4$ and $\theta_1 = \theta_2 = \theta_5 = \theta_6 = 0$) is neither attractive nor repulsive if $\theta_3 \neq 0$.

Proof. (a) follows immediately from (3.3.2.4).

To verify (b)-(c) we consider again discs $b_v, b_{x_1}, b_{x_2}, \ldots$ of equal radii, since it may be possible that Q is degenerate.

We have that $L(b_v \cap \mathcal{U}_{x_1}) > 0 = L(b_v \cap \mathcal{U}_{\emptyset})$ if $b_v \cap b_{x_1} \neq \emptyset$. This provides a simple example where $\lambda_{\theta_2}(\mathbf{x}, v)$ is decreasing or increasing in $\mathbf{x}$ if $\theta_2 > 0$ or $\theta_2 < 0$, respectively. On the other hand, the left panel in Figure 3.2 shows such an example with four discs of equal radii, where the four centers of the discs can be made arbitrary close, and where $L(b_v \cap \mathcal{U}_{\{x_1,x_2,x_3\}}) < L(b_v \cap \mathcal{U}_{\{x_1,x_2\}})$.

Suppose that $b_v \cap b_{x_1} = \emptyset$, $b_v \cap b_{x_2} \neq \emptyset$, and $b_{x_1} \cap b_{x_2} \neq \emptyset$, and let $\mathbf{x} = \{x_1, x_2\}$. Then $\chi(\mathbf{y}, v) = 2$ and $\chi(\mathbf{x}, v) = 1$ if $\mathbf{y} = \{x_1\}$, while $\chi(\mathbf{y}, v) = 1$ and $\chi(\mathbf{x}, v) = 2$ if $\mathbf{y} = \{x_2\}$. Since $\chi = N_{\mathrm{cc}}$ in these examples, we obtain (b) in the case of the χ-interaction process and (c) (i.e. the case of the N_{cc}-interaction process).

Suppose that b_v, b_{x_1}, b_{x_2} have no common intersection but each pair of discs are overlapping, i.e. they form a hole. If $\mathbf{y} = \{x_1, x_2\}$ and the hole disappears when we consider $\mathbf{x} = \{x_1, x_2, x_3\}$, then $N_{\mathrm{h}}(\mathbf{y}, v) = 1$ and $N_{\mathrm{h}}(\mathbf{x}, v) = 0$. Note that $N_{\mathrm{bv}}(\mathbf{y}, v) = 4$ and it may be possible that $N_{\mathrm{bv}}(\mathbf{x}, v) = 2$, as exemplified in the right panel in Figure 3.2. On the other hand, if $\mathbf{y} = \{x_1\}$ and $\mathbf{x} = \{x_1, x_2\}$, then $N_{\mathrm{h}}(\mathbf{y}, v) = 0$, $N_{\mathrm{h}}(\mathbf{x}, v) = 1$, $N_{\mathrm{bv}}(\mathbf{y}, v) = 2$, and $N_{\mathrm{bv}}(\mathbf{x}, v) = 4$. Hence we have established (c) in the case of the N_{h} and N_{bv}-interaction processes.

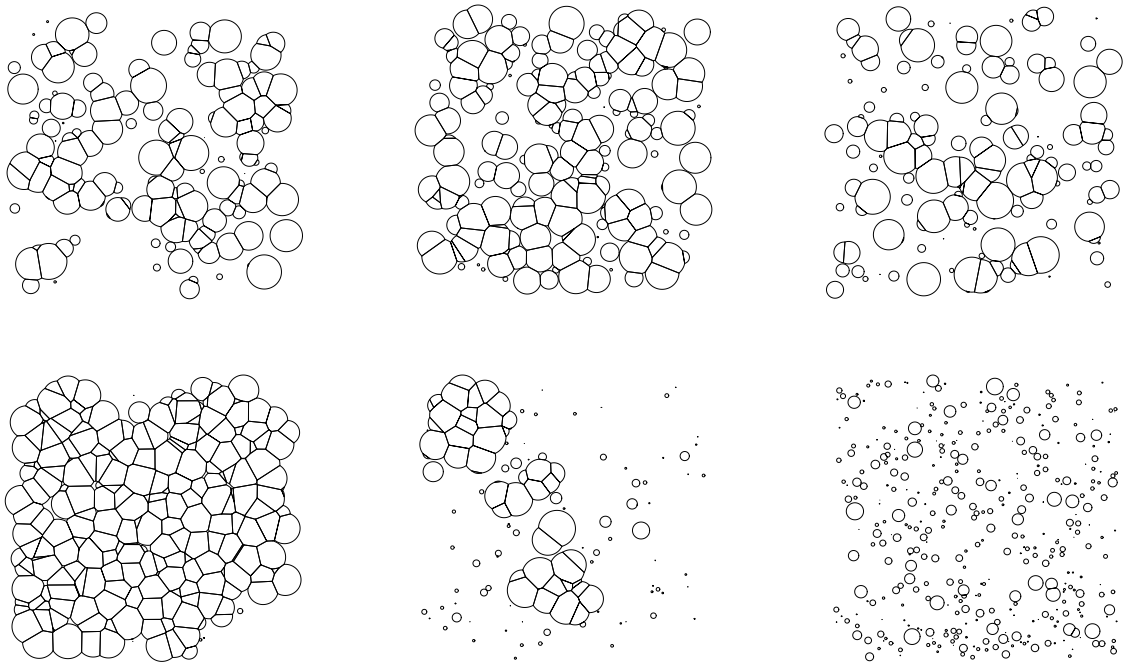

Figure 3.3: Upper line: Simulated realization of the reference Boolean model with Q the uniform distribution on the interval $[0, 2]$, $\rho(u) = 0.2$ on a rectangular region $S = [0, 30] \times [0, 30]$, and $\rho(u) = 0$ outside S (left) and A-interaction model with parameters $\theta_1 = 0.1$ (middle), respective $\theta_1 = -0.1$ (right). Lower line: Simulated realization of (A, L, N_{cc})-interaction process with parameters $(0.6, -1, 1)$ (left), $(0.6, -1, 2)$ (middle) and $(0.6, -1, 5)$ (right).

Finally, the case of the N_{ic}-interaction process in (c) follows simply by considering $\mathbf{x} = x_1$. Then $N_{\mathrm{ic}} = 1$ if $b_u \cap b_{x_1} = \emptyset$ and $N_{\mathrm{ic}} = -1$ otherwise.

□

Thus, in terms of the 'local characteristic' $\lambda_\theta(\mathbf{x}, v)$, we can easily interpret the importance of the parameter θ_1 in the A-interaction process, while the role of the parameters in the other processes is less clear. Their meaning is better understood by simulation studies. Figure 3.3 shows some examples of simulated realizations. In comparison with the reference Boolean model, the A-interaction process with $\theta_1 > 0$ respective $\theta_1 < 0$ tends to produce realizations with a larger respective smaller area $A(\mathcal{U}_{\mathbf{x}})$, and similarly for the G-interaction process with $G = L, \chi, N_{\mathrm{h}}, N_{\mathrm{ic}}, N_{\mathrm{bv}}, N_{\mathrm{cc}}$. However, the interpretation of models with at least two parameters depends on the signs and how large these parameters are, see the lower line of Figure 3.3.

3.3.3 Properties of geometric characteristics

Here, we concern various useful relations between certain geometric characteristics of the union $\mathcal{U}_{\mathbf{x}}$ and of its power tessellation $\mathcal{B}_{\mathbf{x}}$, assuming $\mathbf{x} \in \mathcal{N}^f$. Among other things, the results become useful in connection to computation of geometric characteristics during running the simulations.

Define the following characteristics of $\mathcal{B}_{\mathbf{x}}$:

- the number of non-empty cells $N_{\mathrm{c}} = N_{\mathrm{c}}(\mathcal{B})$,
- the number of interior edges $N_{\mathrm{ie}} = N_{\mathrm{ie}}(\mathcal{B})$,
- the number of edges $N_{\mathrm{e}} = N_{\mathrm{be}} + N_{\mathrm{ie}}$,
- the number of interior vertices $N_{\mathrm{iv}} = N_{\mathrm{iv}}(\mathcal{B})$,
- the number of vertices $N_{\mathrm{v}} = N_{\mathrm{bv}} + N_{\mathrm{iv}}$,
- $N = n(\mathbf{x})$ the number of discs.

Note that these statistics do not appear in the specification (3.3.1.1) since they cannot be determined from $\mathcal{U}$ but only from $\mathcal{B}$.

Lemma 3.3 *We have*

$$N_{\mathrm{ic}} \le N_{\mathrm{cc}} \le N_{\mathrm{c}} \le N, \quad N_{\mathrm{bv}} = 2N_{\mathrm{ie}} - 3N_{\mathrm{iv}} \tag{3.3.3.1}$$

and

$$\chi = N_{\mathrm{cc}} - N_{\mathrm{h}} = N_{\mathrm{c}} - N_{\mathrm{ie}} + N_{\mathrm{iv}}. \tag{3.3.3.2}$$

If $N_{\mathrm{c}} \ge 2$ *and* $N_{\mathrm{cc}} = 1$, *then*

$$N_{\mathrm{be}} = N_{\mathrm{bv}} \le 2N_{\mathrm{ie}}, \quad 3N_{\mathrm{v}} = 2N_{\mathrm{e}}. \tag{3.3.3.3}$$

If $N_{\mathrm{c}} \ge 3$ *and* $N_{\mathrm{cc}} = 1$, *then*

$$N_{\mathrm{ie}} \le 3N_{\mathrm{c}} - 6. \tag{3.3.3.4}$$

Moreover,

$$N_{\mathrm{bv}} \le 6N \tag{3.3.3.5}$$

and

$$N_{\mathrm{h}} = 0 \quad \textit{if } N_{\mathrm{c}} \le 2, \qquad N_{\mathrm{h}} \le 2N_{\mathrm{c}} - 5 \quad \textit{if } N_{\mathrm{c}} \ge 3. \tag{3.3.3.6}$$

Proof. The inequalities in (3.3.3.1) clearly hold, and the identity in (3.3.3.1) follows from a simple counting argument, using that each interior edge has two endpoints, and exactly three interior edges emerge at each interior vertex.

The first identity in (3.3.3.2) is just the definition, and the second identity follows from Euler's formula (see [19]).

Assuming $N_{\mathrm{c}} \geq 2$ and $N_{\mathrm{cc}} = 1$, (3.3.3.3) follows from simple counting arguments, using first that exactly two boundary edges emerge at each boundary vertex, second the simple fact that $N_{\mathrm{bv}} \leq N_{\mathrm{v}}$, and third that exactly three edges emerge at each vertex.

To verify (3.3.3.4), consider the dual graph $\mathcal{D}$. Since we assume that $N_{\mathrm{c}} \geq 3$ and $N_{\mathrm{cc}} = 1$, $\mathcal{D}$ has N_{ie} edges and N_{c} vertices, and so by planar graph theory (see e.g. [20]), since $\mathcal{D}$ is a connected graph without multiple edges, the number of dual edges is bounded by $3N_{\mathrm{c}} - 6$.

To verify (3.3.3.5), note that $N_{\mathrm{bv}} \leq 2N_{\mathrm{ie}}$, cf. (3.3.3.1). Using (3.3.3.4) and considering a sum over all components, we obtain that N_{ie} is bounded above by the number of components with two cells plus three times the number of components with three or more cells. Consequently, $N_{\mathrm{bv}} \leq 6N$.

Finally, to verify (3.3.3.6), note that N_{h} is given by the sum of number of holes of all connected components of $\mathcal{U}$, and a connected component consisting of one or two power cells has no holes, so it suffices to consider the case where $N_{\mathrm{cc}} = 1$ and $N_{\mathrm{c}} \geq 3$. Then by (3.3.3.2), N_{h} is bounded above by $1 - (N_{\mathrm{c}} - N_{\mathrm{ie}})$, which in turn by (3.3.3.4) is bounded above by $2N_{\mathrm{c}} - 5$.

□

Equation (3.3.3.6) is a main result in [11]. Our proof of (3.3.3.6) is much simpler and shorter, demonstrating the usefulness of the power tessellation and its dual graph. The upper bound in (3.3.3.6) can be obtained for any three or more discs: If $\mathbf{x}$ consists of three discs b_1, b_2, b_3 such that $b_i \cap b_j \neq \emptyset$ for $1 \leq i < j \leq 3$ and $b_1 \cap b_2 \cap b_3 = \emptyset$, then $N_{\mathrm{h}} = 1$ and $N_{\mathrm{c}} = 3$, so $N_{\mathrm{h}} = 2N_{\mathrm{c}} - 5$. Furthermore, we may add a fourth, fifth, ... disc, where each added disc generates two new holes—as illustrated in Figure 3.4 in the case of five discs—whereby $N_{\mathrm{c}} = 3, 4, \ldots$ and $N_{\mathrm{h}} = 2N_{\mathrm{c}} - 5$ in each case.

Kendall, van Lieshout and Baddeley [11] noticed the inclusion-exclusion formula for $G = A, L, \chi$:

$$G(\mathcal{U}_{\mathbf{x}}) = \sum_{1}^{n} G(b_i) - \sum_{1 \leq i < j \leq n} G(b_i \cap b_j) + \cdots + (-1)^{n-1} G(b_1 \cap \cdots \cap b_n) \qquad (3.3.3.7)$$

where the sums involve $2^n - 1$ terms. Using the power tessellation, inclusion-exclusion formula with much fewer terms is given by (3.3.3.2) for χ, and by Lemma 3.4 below

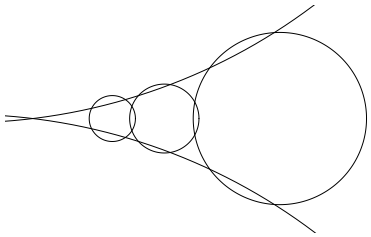

Figure 3.4: A configurations of five discs with exactly $2N_c - 5$ holes.

for A and L. In Lemma 3.4, $I_1(\mathbf{x})$, $I_2(\mathbf{x})$, and $I_3(\mathbf{x})$ denote index sets corresponding to non-empty cells, interior edges, and interior vertices of $\mathcal{B}_\mathbf{x}$, respectively. Note that $I_1(\mathbf{x})$ and $I_2(\mathbf{x})$ correspond to the cliques in the dual graph $\mathcal{D}_\mathbf{x}$ consisting of 1 and 2 nodes, respectively, while $I_3(\mathbf{x})$ corresponds to the subset of 3-cliques $\{i,j,k\} \in \mathcal{D}_\mathbf{x}$ with $b_i \cap b_j \cap b_k \neq \emptyset$ (i.e. $b_i \cup b_j \cup b_k$ has no hole). Note that if $\{i,j,k\} \in \mathcal{D}_\mathbf{x}$, then $b_i \cap b_j \cap b_k \neq \emptyset$ if and only if $E_{i,j} \cap E_{i,k} \neq \emptyset$, where the latter property is easily checked.

Lemma 3.4 *The following inclusion-exclusion formulae hold for the area and perimeter of the union of discs:*

$$A(\mathcal{U}_\mathbf{x}) = \sum_{i \in I_1(\mathbf{x})} A(b_i) - \sum_{\{i,j\} \in I_2(\mathbf{x})} A(b_i \cap b_j) + \sum_{\{i,j,k\} \in I_3(\mathbf{x})} A(b_i \cap b_j \cap b_k) \tag{3.3.3.8}$$

$$= \sum_{i \in I_1(\mathbf{x})} A(B_i) \tag{3.3.3.9}$$

and

$$L(\mathcal{U}_\mathbf{x}) = \sum_{i \in I_1(\mathbf{x})} L(b_i) - \sum_{\{i,j\} \in I_2(\mathbf{x})} L(b_i \cap b_j) + \sum_{\{i,j,k\} \in I_3(\mathbf{x})} L(b_i \cap b_j \cap b_k) \tag{3.3.3.10}$$

$$= \sum_{e \text{ boundary edge of } \mathcal{B}_\mathbf{x}} L(e). \tag{3.3.3.11}$$

Proof. Equations (3.3.3.8) and (3.3.3.10) follow from Theorem 6.2 in [6], while (3.3.3.9) and (3.3.3.11) follow immediately.

□

3.3.4 Markov properties

The various Markov processes considered in this section are either specified by a local Markov property in terms of the Papangelou conditional intensity or by a form of the density given by a Hammersley-Clifford theorem. Particularly, we show that it is useful to

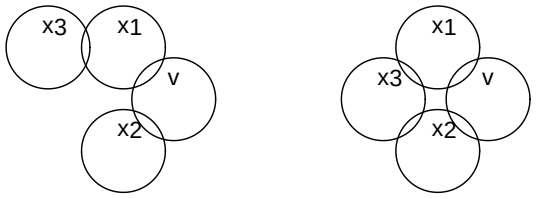

Figure 3.5: An example showing that N_{h}-interaction process is not Markov with respect to the overlap relation: both $N_{\mathrm{h}}(\mathbf{x}, v) = 0$ (left panel) and $N_{\mathrm{h}}(\mathbf{x}, v) = 1$ (right panel) depend on the disc x_3 which is not overlapping the disc v.

view the T-interaction process as a connected component Markov point process, where we show how a spatial Markov property becomes useful for handling edge effects. Throughout this section, we let $\mathbf{x} \in \mathcal{N}^f$.

Markov property in terms of the overlap relation

Consider the overlap relation $\sim$ defined on $S \times (0, \infty)$ by $u \sim v$ if and only if $b(u) \cap b(v) \neq \emptyset$. As introduced in [11], the quermass-interaction process is Markov with respect to $\sim$. The following proposition generalizes this result.

Proposition 3.5 *The T-interaction process with density (3.3.1.2) is Markov with respect to the overlap relation if and only if $\theta_4 = \theta_5 = 0$.*

Proof. Recall that $\lambda(\mathbf{x}, v) = \exp(\theta_1 A(\mathbf{x}, v)) \cdot \exp(\theta_6 N_{\mathrm{bv}}(\mathbf{x}, v))$ It means that we have to verify that the A, L, χ, and N_{bv}-interaction processes are Markov with respect to the overlap relation $\sim$, while the N_{h} and N_{ic}-interaction processes are not Markov. It follows immediately from (3.3.2.4) that the A, L, and χ-interaction processes are Markov. Figures 3.5-3.6 then show that the N_{h} and N_{ic}-interaction processes are not Markov. Further, if w is a boundary vertex of $\mathcal{U}_{\mathbf{x}}$ but not of $\mathcal{U}_{\mathbf{x} \cup \{v\}}$, then w is contained in the disc v. If instead w is a boundary vertex of $\mathcal{U}_{\mathbf{x} \cup \{v\}}$ but not of $\mathcal{U}_{\mathbf{x}}$, then w is given by the intersection of the boundaries of v and an $\mathbf{x}$-disc. Consequently, $N_{\mathrm{bv}}(\mathbf{x}, v) = N_{\mathrm{bv}}(\mathcal{U}_{\mathbf{x} \cup \{v\}}) - N_{\mathrm{bv}}(\mathcal{U}_{\mathbf{x}})$ depends on $\mathbf{x}$ only through $\{u \in \mathbf{x} : u \sim v\}$, so the N_{bv}-interaction process is Markov.

□

Markov property in terms of the connected components

More relevant results for deriving statistical inference in Chapter 4 are Propositions 3.6-3.7 below, where the first proposition states that $\mathbf{X}$ is a connected component Markov

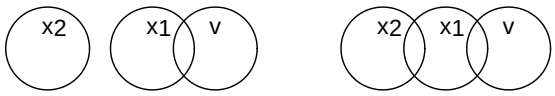

Figure 3.6: An example showing that N_{ic}-interaction process is not Markov with respect to the overlap relation: both $N_{\mathrm{ic}}(\mathbf{x}, v) = -1$ (left panel) and $N_{\mathrm{ic}}(\mathbf{x}, v) = 0$ (right panel) depend on the disc x_2 which is not overlapping the disc v.

process (for more details, see [2]), and the second proposition specifies a spatial Markov property.

Definition 3.13 *The* connected component relation $\sim_{\mathbf{x}}$ *is defined so that for* $u, v \in \mathbf{x}$, $u \sim_{\mathbf{x}} v$ *if and only if* $b(u)$ *and* $b(v)$ *are contained in the same connected component* K *of* $\mathcal{U}_{\mathbf{x}}$.

Definition 3.14 *The process* $\mathbf{X}$ *which is Markov with respect to the connected component relation* $\sim_{\mathbf{x}}$, *is called a* connected component Markov process.

Proposition 3.6 *The* T*-interaction process with density (3.3.1.2) is a connected component Markov point process.*

Proof. The density can be written in the form

$$\frac{1}{c_\theta} \prod_{K \in \mathcal{K}(\mathcal{U}_{\mathbf{x}})} \exp\left(\theta_1 A(K) + \theta_2 L(K) + \theta_3 \chi(K) + \theta_4 N_{\mathrm{h}}(K) + \theta_5 N_{\mathrm{ic}}(K) + \theta_6 N_{\mathrm{bv}}(K)\right) \tag{3.3.4.1}$$

where $\mathcal{K}(\mathcal{U}_{\mathbf{x}})$ is the set of connected components of $\mathcal{U}_{\mathbf{x}}$. Thus, from Hammersley-Clifford theorem, it is a connected component Markov process.

□

Spatial Markov property in terms of the connected component relation

Consider a bounded set $W \subset \mathbb{R}^2$. We split $\mathbf{X}$ into $\mathbf{X}^{(a)}$, $\mathbf{X}^{(b)}$, $\mathbf{X}^{(c)}$ corresponding to discs belonging to connected components of $\mathcal{U}_{\mathbf{X}}$ which are respectively (a) contained in W, (b) intersecting both W and W^c, where W^c denotes the complement of W to $\mathbb{R}^2$, and (c) contained in W^c, see Figure 3.7. Furthermore, let $\mathbf{x}^{(b)}$ denote a realization of $\mathbf{X}^{(b)}$, i.e. $\mathbf{x}^{(b)}$ is a finite configuration of discs such that K intersects both W and W^c for all $K \in \mathcal{K}(\mathcal{U}_{\mathbf{x}^{(b)}})$.

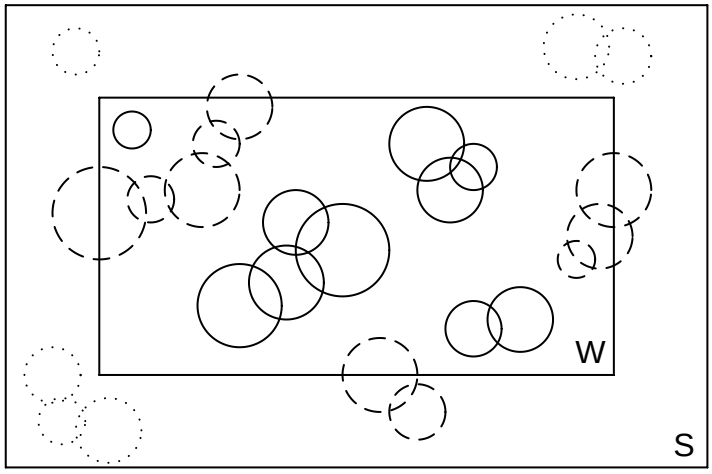

Figure 3.7: Illustrating possible realizations of $\mathbf{X}^{(a)}$ (the full circles), $\mathbf{X}^{(b)}$ (the dashed circles), and $\mathbf{X}^{(c)}$ (the dotted circles).

Proposition 3.7 *Conditional on $\mathbf{X}^{(b)} = \mathbf{x}^{(b)}$, we have that $\mathbf{X}^{(a)}$ and $\mathbf{X}^{(c)}$ are independent, and the conditional distribution of $\mathbf{X}^{(a)}$ depends on $\mathbf{x}^{(b)}$ only through $\mathbf{V} = W \cap \mathcal{U}_{\mathbf{x}^{(b)}}$ and has density*

$$f_\theta(\mathbf{x}^{(a)}|\mathbf{V}) = \frac{1}{c_\theta(\mathbf{V})} \mathbb{I}_{[\mathcal{U}_{\mathbf{x}^{(a)}} \subseteq W \setminus \mathbf{V}]} \exp\left(\theta \cdot T(\mathbf{x}^{(a)})\right) \tag{3.3.4.2}$$

with respect to the reference Boolean model.

Proof. See [14].

□

The density (3.3.4.2) is useful for statistical applications described in Chapter 4, since it accounts for edge effects and depends only on the union of discs intersected by the observation window W. It is a hereditary density of a connected component Markov point process with discs contained in $W \setminus \mathbf{V}$. Its Papangelou conditional intensity $\lambda_\theta(\mathbf{x}^{(a)}, v|\mathbf{V})$ is simply given by

$$\lambda_\theta(\mathbf{x}^{(a)}, v|\mathbf{V}) = \lambda_\theta(\mathbf{x}^{(a)}, v) \mathbb{I}_{[\mathcal{U}_{\mathbf{x}^{(a)} \cup \{v\}} \subseteq W \setminus \mathbf{V}]}. \tag{3.3.4.3}$$

3.3.5 Stability properties

Consider the "unnormalized density" $h_\theta(\mathbf{x}) = \exp(\theta \cdot T(\mathbf{x}))$ corresponding to the T-interaction process with density f_θ given in (3.3.1.2). This section discusses two stability

properties and introduce the condition for c_θ to be finite (i.e. the condition for the density $f_\theta = h_\theta / c_\theta$ to be well-defined).

Ruelle stability

The main question in [11] is to establish Ruelle stability of the quermass-interaction process. The following proposition provides an extension to the general case of the T-interaction process.

Proposition 3.8 *Let*

$$\Theta = \{(\theta_1, \ldots, \theta_6) \in \mathbb{R}^6 : \int \exp\left(\pi\theta_1 r^2 + 2\pi\theta_2 r\right)\, Q(\mathrm{d}r) < \infty\}.$$

For all $\theta \in \Theta$, $c_\theta < \infty$ and f_θ in (3.3.1.2) is a Ruelle stable density. If $\theta \in \mathbb{R}^6 \setminus \Theta$, then $c_\theta = \infty$.

Proof. See [14].

□

Remark 3.7 *Note that $(-\infty, 0]^2 \times \mathbb{R}^4 \subseteq \Theta$, and $\Theta = \mathbb{R}^6$ if supp(Q) is bounded.*

Local stability

Note that a finite product of locally stable functions is a locally stable function, since as mentioned in the proof of Proposition 3.8 its Papangelou conditional intensity is given by a product of Papangelou conditional intensities corresponding to functions $h_{\theta_0}(\mathbf{x}) = \exp(\theta_0 G(\mathcal{U}_\mathbf{x}))$, with $G = A, L, \ldots$ and $\theta_0 = \theta_1, \theta_2, \ldots$.

The fact whether local stability is satisfied or not depends much on how S and supp(Q) are specified. When we in the following proposition write "in general", the proof of the proposition will show examples where local stability is not satisfied.

We let $\epsilon = \inf \mathrm{supp}(Q)$ and $R = \sup \mathrm{supp}(Q)$.

Proposition 3.9 *Local stability is satisfied for*

(a) the A-interaction process if and only if $\theta_1 \leq 0$ or $R < \infty$;

(b) *the L-interaction process if* $\theta_2 = 0$, *or* $R < \infty$ *if* $\theta_2 > 0$, *or* $\epsilon > 0$ *and* $R < \infty$ *if* $\theta_2 < 0$; *otherwise in general it is not locally stable;*

(c) *the* χ*-interaction process if* $\theta_3 \geq 0$, *while in general it is not locally stable if* $\theta_3 < 0$;

(d) *the* N_{cc}*-interaction process if* $\theta_3 = \theta_4 \geq 0$ *or both* $\theta_3 = \theta_4 < 0$ *and* $\epsilon > 0$, *while it is not locally stable if* $\theta_3 = \theta_4 < 0$ *and* $\epsilon = 0$;

(e) *the* N_{ic}*-interaction process if* $\theta_5 \geq 0$ *or* $\epsilon > 0$, *while it is not locally stable if* $\theta_5 < 0$ *and* $\epsilon = 0$.

Moreover, local stability is in general not satisfied for

(f) *the* N_{h}*-interaction process unless* $\theta_4 = 0$;

(g) *the* N_{bv}*-interaction process unless* $\theta_6 = 0$.

Proof. Let $\mathbf{x} \in \mathcal{N}$ and $v \notin \mathbf{x}$.

It follows from (3.3.2.4) that $\lambda_{\theta_1}(\emptyset, v) = \exp(\pi\theta_1 r^2)$, $\lambda_{\theta_1}(\mathbf{x}, v) \leq \exp(\pi\theta_1 r^2)$ if $\theta_1 \geq 0$, and $\lambda_{\theta_1}(\mathbf{x}, v) \leq 1$ if $\theta_1 \leq 0$. Thereby (a) follows, and in a similar way we verify (b) in the case $\theta_2 \geq 0$. It also follows from (3.3.2.4) that the χ-interaction process is locally stable if $\theta_3 \geq 0$.

To verify (b) in the case $\theta_2 < 0$, we suppose first that $\epsilon > 0$ and $R < \infty$. A boundary edge corresponding to an angle $0 < \varphi < 2\pi$ and a disc of radius r has length φr, and it defines a sector of area $\varphi r^2/2$. Since such sectors have disjoint interiors,

$$A(\mathcal{U}_{\mathbf{x}}) \geq \sum_j \varphi_j r_j^2/2 \geq (\epsilon^2/2) \sum_j \varphi_j$$

where the sum is over all boundary edges. Hence

$$L(\mathcal{U}_{\mathbf{x}}) = \sum_j \varphi_j r_j \leq R \sum_j \varphi_j \leq (2R/\epsilon^2) A(\mathcal{U}_{\mathbf{x}}) < c$$

where c is a finite constant (since the discs specified by $\mathbf{x}$ have centers in the bounded region S and their radii are bounded by R, $A(\mathcal{U}_{\mathbf{x}})$ has an upper bound). Consequently,

$$L(\mathbf{x}, v) = L(b_v) - L(b_v \cap \mathcal{U}_{\mathbf{x}}) \geq 2\pi\epsilon - c$$

and so local stability is established when $\theta_2 < 0$, $\epsilon > 0$, and $R < \infty$.

On the other hand, suppose that $\epsilon = 0$ or $R = \infty$. Let r denote the radius of b_v, let $0 < \delta < r$, and consider the infinite configuration of discs of radii δ and centers at the

sites of a equilateral triangular lattice of side length 2δ. The proportion of $\mathbb{R}^2$ covered by these discs is the so-called maximal packing degree $p = \pi/\sqrt{12}$ (a number independent on how δ is chosen). Now, suppose that $\mathbf{x}$ is the subconfiguration of all such discs contained in b_v. As either δ decreases to zero or r increases to infinity, $n(\mathbf{x})\delta^2/r^2$ converges to p, and so

$$L(\mathbf{x}, v) = L(b_v) - L(b_v \cap \mathcal{U}_{\mathbf{x}}) = 2\pi r - 2\pi\delta n(\mathbf{x})$$

is converging to $-\infty$. Hence if $\theta_2 < 0$, the local stability condition is violated, and so (b) is verified.

To show an example where the χ-interaction process is not locally stable if $\theta_3 < 0$, consider Figure 3.8. Suppose $\mathbf{x} = \{x_1, \ldots, x_n\}$ corresponds to the pairwise overlapping small discs in the figure, and b_v to the large disc. Then each pair x_i, x_{i+1} together with b_v form one hole, and $N_{\mathrm{h}}(b_v \cap \mathcal{U}_{\mathbf{x}}) = n - 1$. Since n may be arbitrary large, using again (3.3.2.4), we obtain (c). Notice that b_v does not need to be so large compared to the other discs in Figure 3.8; it is only chosen in this way for illustrative purposes. For example, all the discs may be of a very similar size so that still $N_{\mathrm{h}}(b_v \cap \mathcal{U}_{\mathbf{x}}) = n - 1$ (then the discs in $\mathbf{x}$ will be much more overlapping than indicated in Figure 3.8). More precisely, whether this holds or not depends on how large S is compared to $\mathrm{supp}(Q)$. For instance, if S is a disc with radius R and the discs in the disc process have deterministic radii equal to $2R$, then $\chi(\mathcal{U}_{\mathbf{x}}) = 1$ for all $\mathbf{x} \in \mathcal{N}$, and so the χ-interaction process is locally stable for all $\theta_3 \in \mathbb{R}$.

For (d), we use that

$$N_{\mathrm{cc}}(\mathbf{x}, v) = 1 - \#\{\text{connected components in } \mathcal{U}_{\mathbf{x}} \text{ which are intersected by } b_v\}. \quad (3.3.5.1)$$

Hence we immediately obtain local stability if $\theta_3 = \theta_4 \geq 0$. Suppose instead that $\theta_3 = \theta_4 < 0$. By (3.3.5.1), $N_{\mathrm{cc}}(\mathbf{x}, v)$ has no lower bound if $\epsilon = 0$, since the discs in $\mathbf{x}$ can be disjoint and still all intersect b_v. On the other hand, if $\epsilon > 0$, then $1 - N_{\mathrm{cc}}(\mathbf{x}, v)$ is at most equal to the maximal number of disjoint discs with radius ϵ and centers in S. Thereby (d) is verified. The proof of (e) is similar, using instead that

$$N_{\mathrm{ic}}(\mathbf{x}, v) = \mathbf{1}_{\mathrm{ic}}(\mathbf{x}, v) - \#\{\text{isolated cells in } \mathcal{U}_{\mathbf{x}} \text{ which are contained in } b_v\}$$

where $\mathbf{1}_{\mathrm{ic}}(\mathbf{x}, v)$ is the indicator function which is one if B_v is an isolated cell in $\mathcal{B}_{\mathbf{x}\cup\{v\}}$, and zero otherwise.

The N_{h}-interaction process with $\theta_4 = 0$ and the N_{bv}-interaction process with $\theta_6 = 0$ are nothing but the Boolean model $\mathbf{Y}$, and so local stability is obviously satisfied. By similar arguments as above in the proof of (c) when $\theta_3 < 0$, there are in general no uniform upper and lower bounds on neither $N_{\mathrm{h}}(\mathbf{x}, v)$ nor $N_{\mathrm{bv}}(\mathbf{x}, v)$. Thereby (f) and (g) follow.

□

Note that if the indicator term in (3.3.4.2) is one, it implies that the radius of any disc in $\mathbf{x}^{(a)}$ is less than a constant. Consequently, (a) the conditional A-interaction process given

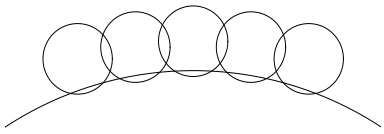

Figure 3.8: A configuration $\mathbf{x}$ of $n = 6$ discs intersected by another disc b_v such that $\#\text{holes}(b_v \cap \mathcal{U}_{\mathbf{x}}) = n - 1 = 5$.

by (3.3.4.2) is always locally stable, and (b) the L-interaction process given by (3.3.4.2) is locally stable if either $\theta_2 \geq 0$ or $\theta_2 < 0$ and $\epsilon > 0$, and in general it is not locally stable if $\theta_2 < 0$ and $\epsilon = 0$.

3.4 Simulations

3.4.1 Metropolis-Hastings algorithm

For simulation of the T-interaction process (3.3.1.2) or the conditional T-interaction process with density (3.3.4.2), we use a simple version of the birth-death type Metropolis-Hastings algorithm studied in [16].

We consider first the T-interaction process $\mathbf{X}$ with Papangelou conditional intensity $\lambda_\theta(\mathbf{x}, v)$ given by (3.3.2.1).

In the Metropolis-Hastings algorithm, if $\mathbf{x}$ is the state at iteration t, we generate a proposal which is either a "birth" $\mathbf{x} \cup \{v\}$ of a new discs $v = (z, r)$ or a "death" $\mathbf{x} \setminus \{x_i\}$ of an old disc $x_i \in \mathbf{x}$. Each proposal may happen with equal probability 1/2. Define

$$H_\theta(\mathbf{x}, v) = \lambda_\theta(\mathbf{x}, v) \frac{\int_S \rho(s)\,\mathrm{d}s}{\rho(z)(n(\mathbf{x}) + 1)}. \tag{3.4.1.1}$$

In case of a birth-proposal, z and r are independent, z has a density on S proportional to ρ, and r follows the distribution Q. This proposal is accepted as the state at iteration $t+1$ with probability $\min\{1, H_\theta^{(1)}(\mathbf{x}, v)\}$, where the Hastings ratio is given by $H_\theta^{(1)}(\mathbf{x}, v) = H_\theta(\mathbf{x}, v)$. In case of a death-proposal, x_i is a uniformly selected point from $\mathbf{x}$, and the Hastings ratio in the acceptance probability $\min\{1, H_\theta^{(2)}\}$ of the proposal is now given by $H_\theta^{(2)}(\mathbf{x}, x_i) = 1/H_\theta(\mathbf{x} \setminus \{x_i\}, x_i)$ (in the special case where $\mathbf{x} = \emptyset$, we do nothing). Finally, if neither one of the proposals is accepted, we retain $\mathbf{x}$ at iteration $t + 1$.

If due to Proposition 3.9, local stability is satisfied, the chain is geometrically ergodic (for more details, see [16]). Moreover, from a computational perspective, the important point

of the algorithm is that it only involves calculating the Papangelou conditional intensity, so only local computations of the statistics appearing in (3.3.2.1) are needed.

It remains to decide when the chain reach the equilibrium (so called *burn-in*). As follows from [16], the suitable method is to consider visually the plots describing the evolution of the geometrical characteristics from T. The burn-in is then establish as the maximal iteration t_{max} such that after the t_{max}-th iteration, values of all the characteristics fluctuate around a fixed value.

In theory, we may use any state of $\mathcal{N}^f$ as the initial state of the algorithm, but we have mainly used three kinds of initial states:

(i) the extreme case of the empty configuration $\emptyset$;

(ii) if local stability is satisfied, the other extreme case is given by a realization from a Poisson process with intensity measure $\beta\rho(z)\,\mathrm{d}z\,Q(\mathrm{d}r)$, where β is the upper bound for Papangelou conditional intensity, i.e. $\lambda_\theta(\mathbf{x}, v) < \beta$;

(iii) a realization of the reference Poisson process $\mathbf{Y}$.

The algorithm for simulating from the conditional processes with density (3.3.4.2) is the same except that we replace $\lambda_\theta(\mathbf{x}, v)$ in (3.4.1.1) by the Papangelou conditional intensity (3.3.4.3). The convergence properties and computations are therefore similar to those discussed above. The initial states are slightly different, where we modify the Poisson process in (ii) or (iii) above so that we first restrict the Poisson process in (ii) or (iii) in order it has centers in W, and second when we make a simulation from this Poisson process, we finally omit those discs which are not included in $W \setminus \mathbf{V}$.

3.4.2 Local calculations

For calculating the area and perimeter, the inclusion-exclusion formulae (3.3.3.9) and (3.3.3.11) appear to be more suited than (3.3.3.8) and (3.3.3.10) when the computations are done in combination with the sequential constructions considered in Sections 3.2.2 and 3.4. Note that we need only to do "local computations".

For example, suppose we are given the power tessellation $\mathcal{B}^{\mathrm{old}}$ of $\mathcal{U}^{\mathrm{old}} = \cup_1^{n-1} b_i$ and add a new disc b_n. When constructing the new power tessellation $\mathcal{B}^{\mathrm{new}}$ of $\mathcal{U}^{\mathrm{new}} = \cup_1^{n} b_i$, we need only to consider the new set B_n and the old cells in $\mathcal{B}^{\mathrm{old}}$ which are neighbours to B_n with respect to the dual graph of $\mathcal{B}^{\mathrm{new}}$ (see the first part of Section 3.2.2). Similarly, when a disc is deleted and the new tessellation is constructed, we need only local computations with respect to the discs intersecting the disc which is deleted (see the second part of

Section 3.2.2). Moreover, only local computations are needed also when calculating N_{ic} and N_{bv}.

Finally, we explain in more detail how we can find the area A. We can easily determine the total area of all isolated cells of $\mathcal{B}$. Suppose that B_i is a non-empty, non-isolated cell of $\mathcal{B}$. Let c_i denote the arithmetic average of the vertices of B_i. Then $c_i \in B_i$, since B_i is convex. For any three points $c, u, v \in \mathbb{R}^2$, let $\Delta(c, u, v)$ denote the triangle with vertices c, u, v. If $\lfloor u, v \rceil$ is a boundary edge of B_i, let $\Gamma(u, v)$ denote the cap of b_i bounded by the arc $\lfloor u, v \rceil$ and the line segment $[u, v]$. Then the area of B_i is the sum of areas of all triangles $\Delta(c_i, u, v)$, where u and v define an (interior or boundary) edge of B_i, plus the sum of areas of all caps $\Gamma(u, v)$, where u and v define a boundary edge of B_i.

Chapter 4

Statistical Inference

4.1 Basic problems and their solutions

In this chapter, we will use the notation $\mathbf{D}$ for the data and $W \subset \mathbb{R}^2$ for a bounded observation window.

Statistical inference of a random closed set given by a union of discs is often complicated by the following facts:

(i) as we observe only the union and not the discs themselves, the individual grains may be (and usually are) unobservable,

(ii) since we observe only $\mathbf{D} \cap W$, edge effects may occur,

(iii) in practice the grains may only approximately be discs,

(iv) usually only a digital image is observed and the resolution makes it difficult to identify circular structures.

Fitting the model described in Chapter 3 to the data, the first problem is solved, since the geometrical characteristics in the density depend only on the whole union $\mathcal{U}$, not on the size or number of individual discs. The second complication will be studied in details later in Section 4.3. The problems (iii) and (iv) can be solved by modifying the density (3.3.1.2) to the form

$$f_\theta(\mathbf{x}) = \frac{1}{c_\theta} \exp\left(\theta_1 A(\mathcal{U}_\mathbf{x}) + \theta_2 L(\mathcal{U}_\mathbf{x}) + \theta_3 N_{\mathrm{cc}}(\mathcal{U}_\mathbf{x}) + \theta_4 N_{\mathrm{h}}(\mathcal{U}_\mathbf{x})\right). \tag{4.1.0.1}$$

This modification means that we omit the characteristics N_{ic} and N_{bv} which usually cannot be clearly identified in the image, and we keep the remaining four characteristics,

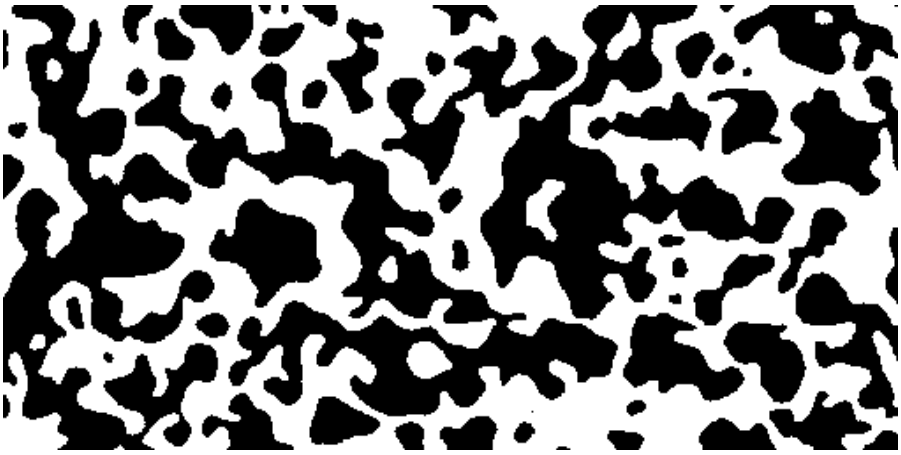

Figure 4.1: The heather dataset.

where we replace the couple of characteristics (χ, N_{h}) by $(N_{\mathrm{cc}}, N_{\mathrm{h}})$ because the meaning of these two characteristics is better convertible. Thus, for the rest of this chapter, we will work with statistic

$$T = (A, L, N_{\mathrm{cc}}, N_{\mathrm{h}}). \tag{4.1.0.2}$$

4.2 Data and previous analyses

As an application example, we consider the well known heather dataset first presented in [4] shown in Figure 4.1 as a binary image of the presence of heather (*Calluna vulgaris*, indicated by black) in a 10×20 m rectangular region W at Jädraås, Sweden. Assuming the heather plants form approximately hemispherical bushes, we identify heather bushes (or more precisely, their two-dimensional projection) and discs.

Remark 4.1 *While the dataset in Diggle (1981) was coded as a* 100×200 *binary matrix, Figure 4.1 consists of* 250×508 *pixels.*

Diggle (1981) modeled the presence of heather by a stationary random-disc Boolean model. Let R denote a typical disc radius, where units are meters. Diggle modeled its distribution by a three-parameter Weibull distribution

$$\kappa\alpha(r-\delta)^{\kappa-1} \exp\left(-\alpha(r-\delta)^{\kappa}\right), \quad r \geq \delta \tag{4.2.0.3}$$

where δ, κ, α are positive parameters. He estimated the parameters by a minimum contrast method based on the covariance function for the indicator function of presence

of heather, splitting the 10×20 m window W into two 10×10 m non-overlapping squares in order to compare the obtained results. His estimates of $(\rho, \delta, \kappa, \alpha)$ were $(2.21, 0.281, 0.281, 20.6)$ for the left-hand square, and $(2.11, 0.226, 1.011, 12.5)$ for the right-hand square, corresponding to a mean and standard deviation of R of approximately 0.31 and 0.04 (left-hand square) and 0.31 and 0.08 (right-hand square), and an intensity of around two bushes per square meter.

This procedure passed a model validation introduced in [4] based on the spherical contact distribution function, however, as Diggle pointed out after comparing simulation of the fitted models with the data, the visual impression is not good, since the fitted models generate more separate patches than the data. Later, Hall in [7] noticed that Diggle's estimates of radius standard deviation may be too small. Then, in [18], there are constructed tools for valuation of the shape of the random set based on operations defined in Section 4.6 of this work which also indicated that Diggle's random-disc Boolean model is not fitting well. Finally, Hall in [8] noticed that some of the differences between data and fitted models would diminish if the discs were given ragged edges.

Hall in [8] then considered a stationary Boolean model with germ intensity ρ and isotropic convex grains $\mathbf{K}$, and assumed that $\mu_1 = \mathrm{E}\left[L(\mathbf{K})\right]/(2\pi)$ and $\mu_2 = \mathrm{E}\left[A(\mathbf{K})\right]/\pi$ (note that for a stationary Boolean model with circular grains, $\mu_i = \mathrm{E}(R^i)$, $i = 1, 2$, i.e. $\mu = \mu_1$ is the mean and $\sigma = \sqrt{\mu_2 - \mu^2}$ the standard deviation of R) are finite. Using that the number of grains intersecting a fixed convex set C is Poisson distributed with mean $\rho(A(C) + L(C)\mu_1 + \pi\mu_2)$, and using a quadratic lattice with C corresponding to an arbitrary vertex, edge, or square, he derived moment equations from which estimates of ρ, μ_1, μ_2 were obtained (this procedure is considered in Section 4.4 in connection to (4.4.0.3)). The estimate of ρ was approximately equal to 2.36, and taking bushes to be discs, estimates of about 0.27 m and 0.12 m for μ and σ, respectively, were calculated.

Further approaches of fitting Boolean model can be found in [3], where the primary aim was to estimate ρ using Laslett's transformation which transforms the exposed marker points (for a convex grain, the marker point is the most southwesterly point of the grain) into a stationary Poisson process of intensity ρ. He obtained the estimate 1.16 of ρ which is much lower value than that obtained by the previous analyses. It is explained by Cressie so that this discrepancy may be partly caused by missing exposed marker points due to the digitization of the image of heather data.

4.3 MCMC maximum likelihood

Using MCMC methods, approximate maximum likelihood estimates of the parameter θ from (4.1.0.1) can be obtained. Sections 4.3.1 and 4.3.2 specify two likelihood functions which solve the edge effects problem in different ways.

In general, the MCMC maximum likelihood method works as follows. Note that writing the density in the form $f_\theta(\mathbf{x}) = h_\theta(\mathbf{x})/c_\theta$ (i.e. $h_\theta(\mathbf{x}) = \exp(\theta \cdot T(\mathcal{U}_\mathbf{x}))$ is the unnormalized density), the log likelihood function for an observation $\mathbf{x}$ (or better say for an observation $\mathcal{U}_\mathbf{x}$ as we observe only the whole union) is given by

$$L(\theta) = \log h_\theta(\mathbf{x}) - \log c_\theta = \theta \cdot T(\mathcal{U}_\mathbf{x}) - \log c_\theta.$$

However, as mentioned in Section 3.1.1, we have no explicit expression for c_θ. Therefore it is easier to maximize the log likelihood ratio

$$L(\theta) - L(\theta_0) = \log(h_\theta(\mathbf{x})/h_{\theta_0}(\mathbf{x})) - \log(c_\theta/c_{\theta_0}) \tag{4.3.0.4}$$

for fixed θ_0 instead, because c_θ/c_{θ_0} can be approximated by

$$\frac{1}{n}\sum_{m=0}^{n-1} h_\theta(\mathbf{Z}_m)/h_{\theta_0}(\mathbf{Z}_m),$$

where $\mathbf{Z}_m$ are realizations from $f_{\theta_0}(\mathbf{x})$ which can be obtained by MCMC simulations described in Section 3.4.

For maximising (4.3.0.4), we use Newton-Raphson method working in two following steps:

1. Set $\hat{\theta}^{(0)} = \theta_0$;
2. $(k+1)$-th iteration is given by

$$\hat{\theta}^{(k+1)} = \hat{\theta}^{(k)} + u_{\theta_0,n}(\hat{\theta}^{(k)}) j_{\theta_0,n}(\hat{\theta}^{(k)})^{-1},$$

where

$$u_{\theta_0,n}(\hat{\theta}^{(k)}) = T(\mathcal{U}_\mathbf{x}) - \mathbb{E}_{\hat{\theta}^{(k)},\theta_0,n} T(\mathcal{U}_\mathbf{X}) \tag{4.3.0.5}$$

$$= T(\mathcal{U}_\mathbf{x}) - \frac{\sum_{m=0}^{n-1} T(\mathcal{U}_{\mathbf{Z}_m}) h_{\hat{\theta}^{(k)}}(\mathbf{Z}_m)/h_{\theta_0}(\mathbf{Z}_m)}{\sum_{m=0}^{n-1} h_{\hat{\theta}^{(k)}}(\mathbf{Z}_m)/h_{\theta_0}(\mathbf{Z}_m)} \tag{4.3.0.6}$$

and analogously

$$j_{\theta_0,n}(\hat{\theta}^{(k)}) = \mathbb{V}\mathrm{ar}_{\hat{\theta}^{(k)},\theta_0,n} T(\mathcal{U}_\mathbf{X}) \tag{4.3.0.7}$$

$$= \frac{\sum_{m=0}^{n-1} (T(\mathcal{U}_{\mathbf{Z}_m}) - \mathbb{E}_{\hat{\theta}^{(k)},\theta_0,n} T(\mathcal{U}_\mathbf{X}))^2 h_{\hat{\theta}^{(k)}}(\mathbf{Z}_m)/h_{\theta_0}(\mathbf{Z}_m)}{\sum_{m=0}^{n-1} h_{\hat{\theta}^{(k)}}(\mathbf{Z}_m)/h_{\theta_0}(\mathbf{Z}_m)}. \tag{4.3.0.8}$$

This gradient algorithm converges very fast in the sense that after few iterations, the obtained estimates do not change with increasing number of the iterations. The concrete values of the number of needed iterations together with the number of needed simulations n are specified in Section 4.5.

4.3.1 Conditional likelihood

Recall that when we split the disc process $\mathbf{X}$ into $\mathbf{X}^{(a)}$, $\mathbf{X}^{(b)}$, $\mathbf{X}^{(c)}$ corresponding to discs belonging to connected components of $\mathcal{U}_{\mathbf{X}}$ which are respectively contained in W, intersecting both W and W^c, and contained in W^c (Figure 3.7), then the conditional distribution of $\mathbf{X}^{(a)}$ depends on the realization $\mathbf{x}^{(b)}$ of $\mathbf{X}^{(b)}$ only through $\mathbf{V} = W \cap \mathcal{U}_{\mathbf{x}^{(b)}}$. Practically, it means that the conditional density (3.3.4.2) depends only on something we can observe (namely $\mathbf{V}$) and it does not depend on how we choose S. Therefore, we consider the conditional log likelihood

$$L_c(\theta) = \theta \cdot T(\mathcal{U}_{\mathbf{x}^{(a)}}) - \log c_\theta(\mathbf{V}) \tag{4.3.1.1}$$

corresponding to the conditional density (3.3.4.2), where $\mathbf{x}^{(a)}$ denotes a realization of the process $\mathbf{X}^{(a)}$.

For the heather data, Figure 4.2 shows the connected components intersecting the boundary of W (in gray). We denote the union of these components by $\mathbf{D}^{(b)}$ and set $\mathbf{D}^{(a)} = (\mathbf{D} \cap W) \setminus \mathbf{D}^{(b)}$. In (4.3.1.1) we use the approximations $\mathbf{D}^{(a)} \approx \mathcal{U}_{\mathbf{x}^{(a)}}$ and $\mathbf{D}^{(b)} \approx \mathbf{V}$, where

$$A(\mathbf{D}^{(a)}) = 45.6, \quad L(\mathbf{D}^{(a)}) = 190, \quad N_{\mathrm{cc}}(\mathbf{D}^{(a)}) = 32, \quad N_{\mathrm{h}}(\mathbf{D}^{(a)}) = 2. \tag{4.3.1.2}$$

The perimeter was calculated by a method based on intrinsic volume densities (for more details, see [17], and for software, see `http://home.pf.jcu.cz/~mrkvicka/math/`), while the values of the three other characteristics were easily determined.

Remark 4.2 *Note that* $A(\mathbf{V})/A(W) = 0.2734$. *When we compare it to* $A(\mathbf{D} \cap W)/A(W) = 0.5014$, *it is seen that there is a loss of information.*

4.3.2 Unconditional likelihood

In some applications it may happen that $\mathbf{D}^{(a)} = \emptyset$, in which case the maximum likelihood estimate based on (4.3.1.1) has no sense. Partly for this reason and partly for comparison to the conditional maximum likelihood approach based on (4.3.1.1), we also consider the following unconditional approach. Though we know that the heather grow lives outside W, we suppose that $S = W$, let $\tilde{\mathbf{D}} = \mathbf{D} \cap W$, and approximate the log likelihood by

$$\begin{aligned} L_u(\theta) &= \theta \cdot T(\tilde{\mathbf{D}}) - \log c_\theta \\ &= \theta_1 A(\tilde{\mathbf{D}}) + \theta_2 L(\tilde{\mathbf{D}}) + \theta_3 N_{\mathrm{cc}}(\tilde{\mathbf{D}}) + \theta_4 N_{\mathrm{h}}(\tilde{\mathbf{D}}) - \log c_\theta \end{aligned} \tag{4.3.2.1}$$

where

$$A(\tilde{\mathbf{D}}) = 100.28, \quad L(\tilde{\mathbf{D}}) = 382.82, \quad N_{\mathrm{cc}}(\tilde{\mathbf{D}}) = 56, \quad N_{\mathrm{h}}(\tilde{\mathbf{D}}) = 6. \tag{4.3.2.2}$$

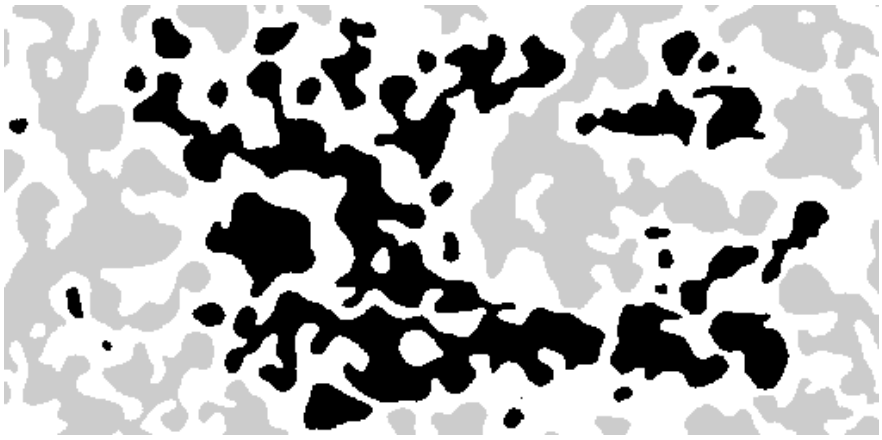

Figure 4.2: Heather dataset with the components intersecting the boundary of the observation window coloured gray.

Even when we assume $S = W$, some edge effects occur, since compared to (3.1.1.1) we have replaced $\mathcal{U}_{\mathbf{x}}$ by $\tilde{\mathbf{D}}$, although $\mathcal{U}_{\mathbf{x}}$ expands outside W. Moreover, for convenience we use the normalizing constant c_θ from (3.1.1.1) with $S = W$ and approximate it again by MCMC methods as described at the beginning of Section 4.3.

4.4 Reference processes

Except two types of likelihood, we compare also results obtained for three different reference Boolean models which are specified by (R1)-(R3) below. Note that the normalizing constants in the density (3.3.1.2), the conditional likelihood (4.3.1.1) and the unconditional likelihood (4.3.2.1) depend on the choice of reference process.

In the sequel we assume that the radii distriburion R has bounded support which implies that $\mathbf{\Theta} = \mathbb{R}^4$ is as large as possible (see Proposition 3.8). Independent biological evidence suggests that R should be less than 0.5 m (see [4]) which is significant information for choice of the upper boundary of R.

The remaining parameters for the reference processes are obtained by a method from [7]. For this method, we use a square lattice, and after some experimentation we decided to work with the side length $c_1 = 0.48$ m (i.e. a square roughly corresponds to 12×12 pixels in Figure 4.1 where 1 pixel corresponds to 4×3.94 cm). Within W, the lattice has $n_0 = 903$ vertices, $n_1 = 1742$ edges, and $n_2 = 840$ squares. Denote $(N_0, N_1, N_2) = (450, 474, 71)$ the numbers of these vertices, edges, and squares which are not intersected by $\mathbf{D}$. Let $A_i = \log(n_i/N_i)$, $i = 0, 1, 2$, and let $c_2 = c_1^2 = 0.2304$ m^2 be the area of a square. By Hall's

method, the estimates of the intensity ρ and the first two moments $\mu_i = \mathbb{E}R^i$, $i = 1, 2$, of the radii distribution R are given by

$$\rho = \frac{1}{c_2}\left(A_0 - 2A_1 + A_2\right), \quad \mu_1 = \frac{1}{2c_1\rho}\left(A_1 - A_0\right), \quad \mu_2 = \frac{A_0}{\pi\rho}. \tag{4.4.0.3}$$

We obtain $(2.45, 0.26, 0.09)$ as the estimate of (ρ, μ_1, μ_2), and hence $(0.26, 0.16)$ as the estimate of the mean and the standard deviation (μ, σ).

Remark 4.3 *Our estimate of (ρ, μ, σ) is slightly different from that obtained by Hall in [8] because we worked with a different lattice and another resolution of the image.*

Taking $\mu = 0.26$ and $\sigma = 0.16$ from as introduced above together with the information about upper boundary for the discs radii, the three reference Boolean models are specified by

(R1) $\rho = 2.45$ and R follows the restriction of $N(\mu, \sigma^2)$ to the interval $[0, 0.50]$;

(R2) $\rho = 2.45$ and R is uniformly distributed on $[0, 0.53]$;

(R3) $\rho = 1.16$ and R is uniformly distributed on $[0, 0.53]$.

Normal and uniform distributions are considered because of their easy simulation. Moreover, a normal distribution has also been considered in [8]. The restriction of $N(\mu, \sigma^2)$ to the interval $[0, 0.50]$ corresponds to 88 % of the probability mass. Under (R1), the mean of R is close to μ, and its standard deviation is 0.12 which are values close to the estimates of the mean and standard deviation obtained in [7]. Under both (R2) and (R3), R has approximately the estimated mean $\mu = 0.26$ and the standard deviation $\sigma = 0.16$.

Remark 4.4 *Note that the exact interval for uniformly distributed random variable with $\mu = 0.26$ and $\sigma = 0.16$ is $[-0.01, 0.53]$, but naturally, we consider only the positive values of R.*

For random-disc Boolean models, the area fraction is given by

$$p = 1 - \exp(-\rho\pi(\sigma^2 + \mu^2)), \tag{4.4.0.4}$$

hence the area fraction is $p = 0.46$ under (R1), $p = 0.51$ under (R2), and $p = 0.29$ under (R3). For comparison, the empirical area fraction is $\hat{p} = 0.5014$. The small area fraction under (R3) is caused by the small value of $\rho = 1.16$ taken from [12], cf. Section 4.2.

4.5 Numerical results

This section discusses simulation-based inference where first in Section 4.5.1 we compare the results obtained by using the conditional likelihood $L_c(\theta)$ for the different reference processes (R1)-(R3) from Section 4.4. Section 4.5.2 then compares these results with other ones based on the unconditional likelihood $L_u(\theta)$. When we have maximum likelihood estimates, we derive also confidence intervals, Wald statistics and p-values following from the Wald test. Section 4.5.3 then compares the intensities of the discs and their radii distributions for the model under (R1)-(R3).

For the simulations we use the Metropolis-Hastings birth-death algorithm discussed in Section 3.4 with a burn-in of 10^4 simulations and samples for MCMC estimates based on 10^6 simulations. Further, we use 30 iterations for Newton-Raphson method.

4.5.1 Numerical results based on the conditional likelihood

Maximum likelihood estimates (MLE) based on $L_c(\theta)$ under the full model $\theta \in \mathbb{R}^4$ for each of the reference processes (R1)-(R3) were obtained by the procedure described in Section 4.3.

The obtained estimates were further tested by Wald test whether they can be considered to be equal to zero. Wald test is generally used for testing the hypothesis $H : \theta M = 0$, where M is a $d \times k$ matrix of the rank k and d is the dimension of the vector T (i.e. $d = 4$ in our case). Using the notation from Section 4.3, i.e. $j(\hat{\theta})$ denotes the variance matrix of the characteristics $(A, L, N_{\mathrm{cc}}, N_{\mathrm{h}})$ in the model with the density $f_{\hat{\theta}}$, Wald statistic

$$(\hat{\theta}M)(M^T j(\hat{\theta})^{-1} M)(\hat{\theta}M)^T$$

is asymptotically χ^2_k-distributed. Obviously, it holds that

$$H' : \theta_i = 0 \iff H : \theta M = 0,$$

where M is 4×1 matrix with all elements equal to zero except the i-th element which is equal to a nonzero constant, say e.g. 1. Thus, we use this test with such a matrix M for testing the parameters θ_i, $i = 1, \ldots, 4$.

Moreover, since $(\hat{\theta} - \theta) j(\hat{\theta})^{1/2}$ is asymptotically $N_d(0, I)$ distributed (see [16]), we are able to establish the confidence intervals for the value of true parameters.

The estimated parameters together with the corresponding 95% confindence intervals, Wald statistics and p-values obtained from Wald test are shown in Table 4.1.

	θ_1	θ_2	θ_3	θ_4
(R1)	-2.14	0.89	-1.78	$\mathbf{-1.01}$
95%-CI	$[-3.68, -0.60]$	$[0.48, 1.31]$	$[-2.28, -1.28]$	$[\mathbf{-2.37}, \mathbf{0.34}]$
Wald	7.45	17.89	48.96	$\mathbf{2.14}$
p-value	0.0063	$2.3 \cdot 10^{-5}$	$2.6 \cdot 10^{-12}$	$\mathbf{0.1435}$
(R2)	-4.81	1.17	-2.26	$\mathbf{-0.69}$
95%-CI	$[-6.36, -3.26]$	$[0.75, 1.58]$	$[-2.74, -1.77]$	$[\mathbf{-2.04}, \mathbf{0.66}]$
Wald	37.04	29.77	83.66	$\mathbf{1.01}$
p-value	$1.2 \cdot 10^{-9}$	$4.9 \cdot 10^{-8}$	$< 10^{-16}$	$\mathbf{0.3149}$
(R3)	-3.67	1.62	-2.25	$\mathbf{-0.13}$
95%-CI	$[-5.42, -1.93]$	$[1.16, 2.09]$	$[-2.76, -1.73]$	$[\mathbf{-1.49}, \mathbf{1.23}]$
Wald	17.01	46.67	73.01	$\mathbf{0.04}$
p-value	$3.7 \cdot 10^{-5}$	$8.4 \cdot 10^{-12}$	$< 10^{-16}$	$\mathbf{0.8415}$

Table 4.1: Under the full model (i.e. $(\theta_1, \theta_2, \theta_3, \theta_4) \in \mathbb{R}^4$), when using each of the reference processes (R1)-(R3), the table shows MLE's based on conditional likelihood L_c and 95%-confidence intervals together with Wald statistics and p-values for testing each of the four hypotheses $\theta_i = 0$ with $i = 1, 2, 3, 4$.

	θ_1	θ_2	θ_3
(R1)	-2.33	0.92	-1.77
95%-CI	$[-3.80, -0.85]$	$[0.52, 1.31]$	$[-2.27, -1.26]$
Wald	9.54	21.01	46.89
p-value	0.0020	$4.6e \cdot 10^{-6}$	$7.5 \cdot 10^{-12}$
(R2)	-4.91	1.18	-2.25
95%-CI	$[-6.48, -3.35]$	$[0.77, 1.59]$	$[-2.75, -1.75]$
Wald	38.02	32.33	78.78
p-value	$7.0 \cdot 10^{-10}$	$1.3 \cdot 10^{-8}$	$< 10^{-16}$
(R3)	-3.71	1.64	-2.25
95%-CI	$[-5.47, -1.95]$	$[1.17, 2.10]$	$[-2.77, -1.74]$
Wald	17.04	47.11	73.89
p-value	$3.7 \cdot 10^{-5}$	$6.7 \cdot 10^{-12}$	$< 10^{-16}$

Table 4.2: Under the reduced model (i.e. $(\theta_1, \theta_2, \theta_3) \in \mathbb{R}^3$ and $\theta_4 = 0$), when using each of the reference processes (R1)-(R3), the table shows MLE's based on conditional likelihood L_c and 95%-confidence intervals together with Wald statistics and p-values for testing each of the three hypotheses $\theta_i = 0$ with $i = 1, 2, 3$.

As seen from Table 4.1, the first three parameters seems to be significant for the model while θ_4 was rather denoted to be equal to zero. Therefore we reduce the model so that we omit the paramater θ_4 from the density (4.1.0.1) and replace it by the density

$$f_\theta(\mathbf{x}) = \frac{1}{c_\theta} \exp\left(\theta_1 A(\mathcal{U}_\mathbf{x}) + \theta_2 L(\mathcal{U}_\mathbf{x}) + \theta_3 N_{\mathrm{cc}}(\mathcal{U}_\mathbf{x})\right). \tag{4.5.1.1}$$

For this reduced model, we again use the procedure described above. The newly obtained estimates, confidence intervals, Wald statistics ad p-values are shown in Table 4.2.

4.5.2 Numerical results based on the unconditional likelihood

As shown in Table 4.3 and Table 4.4 a little bit different conclusions are obtained when inference is based on the unconditional likelihood L_u in (4.3.2.1).

Since the heather plants live outside W and the conditional likelihood L_c accounts for edge effects, while the consequence of ignoring edge effects and use L_u is unclear we prefer to base inference on the conditional likelihood. Thus, the following results presented in this work are shown only for the (A, L, N_{cc})-interaction models with parameters obtained by conditional likelihood and we only note that the statistical inference based on unconditional likelihood which is not presented in this work is very similar to them.

	θ_1	θ_2	θ_3	θ_4
(R1)	$\mathbf{-0.52}$	$\mathbf{-0.10}$	-1.11	-0.91
95%-CI	$[\mathbf{-1.53}, \mathbf{0.50}]$	$[\mathbf{-0.39}, \mathbf{0.19}]$	$[-1.47, -0.75]$	$[-1.68, -0.14]$
Wald	$\mathbf{1.01}$	$\mathbf{0.44}$	35.88	5.41
p-value	$\mathbf{0.3149}$	$\mathbf{0.5071}$	$2.1 \cdot 10^{-9}$	0.0200
(R2)	-3.32	0.72	-1.62	$\mathbf{-0.49}$
95%-CI	$[-4.27, -2.36]$	$[0.44, 1.00]$	$[-1.96, -1.27]$	$[\mathbf{-1.28}, \mathbf{0.29}]$
Wald	46.29	25.72	85.27	$\mathbf{1.50}$
p-value	$1.0 \cdot 10^{-11}$	$3.9 \cdot 10^{-7}$	$< 10^{-16}$	$\mathbf{0.2207}$
(R3)	-1.79	1.04	-1.64	$\mathbf{0.01}$
95%-CI	$[-2.93, -0.64]$	$[0.71, 1.37]$	$[-2.02, -1.25]$	$[\mathbf{-0.78}, \mathbf{0.79}]$
Wald	9.38	37.63	67.85	$\mathbf{0.00}$
p-value	0.0022	$8.6 \cdot 10^{-10}$	$2.2 \cdot 10^{-16}$	$\mathbf{1}$

Table 4.3: Under the full model (i.e. $(\theta_1, \theta_2, \theta_3, \theta_4) \in \mathbb{R}^4$), when using each of the reference processes (R1)-(R3), the table shows MLE's based on unconditional likelihood L_u and 95%-confidence intervals together with Wald statistics and p-values for testing each of the four hypotheses $\theta_i = 0$ with $i = 1, 2, 3, 4$.

	θ_1	θ_2	θ_3
(R1)	$\mathbf{-0.91}$	$\mathbf{-0.02}$	-1.13
95%-CI	$[\mathbf{-1.83, 0.00}]$	$[\mathbf{-0.29, 0.25}]$	$[-1.49, -0.78]$
Wald	$\mathbf{3.80}$	$\mathbf{0.02}$	39.25
p-value	$\mathbf{0.0512}$	$\mathbf{0.8875}$	$3.7e \cdot 10^{-10}$
(R2)	-1.75	1.02	-1.63
95%-CI	$[-2.85, -0.65]$	$[0.70, 1.34]$	$[-2.01, -1.25]$
Wald	9.70	39.65	70.81
p-value	0.0018	$3.08 \cdot 10^{-10}$	$< 10^{-16}$
(R3)	-3.45	0.74	-1.63
95%-CI	$[-4.41, -2.48]$	$[0.46, 1.01]$	$[-1.98, -1.28]$
Wald	49.35	26.82	82.86
p-value	$2.1 \cdot 10^{-12}$	$2.2 \cdot 10^{-7}$	$< 10^{-16}$

Table 4.4: Under the reduced model (i.e. $(\theta_1, \theta_2, \theta_3) \in \mathbb{R}^3$ and $\theta_4 = 0$), when using each of the reference processes (R1)-(R3), the table shows MLE's based on unconditional likelihood L_u and 95%-confidence intervals together with Wald statistics and p-values for testing each of the three hypotheses $\theta_i = 0$ with $i = 1, 2, 3$.

4.5.3 Intensity of the grains and their radii distribution

In Section 4.2, we reported on various results for the mean and variance of the typical radius R and the intensity of bushes as obtained by Diggle and Hall. For comparison with these results, Table 4.5 summaries the results obtained by our estimated (A, L, N_{cc})-interaction models, and Figure 4.3 shows the estimated distributions of the typical radius R together with the densities of the typical radius under the corresponding reference processes.

Table 4.5 shows that the estimated intensities under the fitted (A, L, N_{cc})-interaction models with reference processes (R1) and (R2) are rather close, while the estimated intensity seems to be too small in the case where (R3) is the reference process, probably because ρ is too small in that case. The mean and standard deviation of R are very similar for all three fitted (A, L, N_{cc})-interaction models and close to the results obtained in [8]. However, while our conclusions earlier have been rather independent on the choice of reference process, the distributions in Figure 4.3 are sensitive to this choice. In the case where (R1) is the reference process, there is a rather close agreement between the distributions of R under (R1) and the fitted (A, L, N_{cc})-interaction model, while the disagreement is pronounced in the two other cases. Moreover, the low intensity of discs under the fitted (A, L, N_{cc})-interaction model in the case when (R3) is the reference process may effect the law of R which seems to prefer discs with larger radii.

The distribution of R was estimated as follows. For each of the fitted (A, L, N_{cc})-

	(R1)	(R2)	(R3)
mean of R	0.28	0.25	0.28
sd of R	0.12	0.13	0.13
intensity	2.57	2.36	1.76

Table 4.5: Under the reduced model (i.e. $(\theta_1, \theta_2, \theta_3) \in \mathbb{R}^3$ and $\theta_4 = 0$), when using each of the reference processes (R1)-(R3), the table shows MCMC estimates of the mean and standard deviation of the typical radius and intensity of bushes.

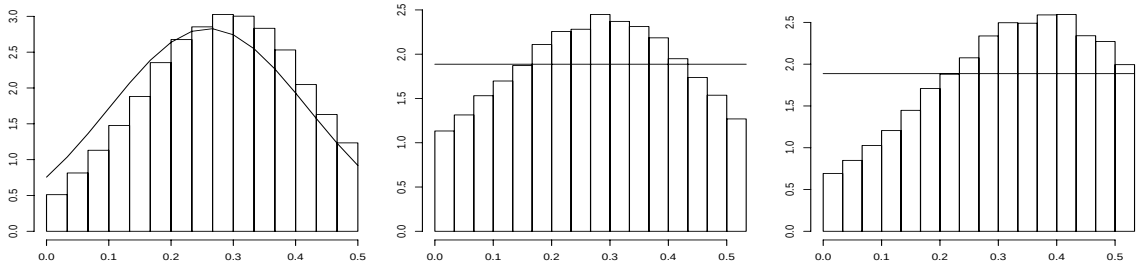

Figure 4.3: Estimated distribution of the typical radius under the fitted (A, L, N_{cc})-interaction models with parameters as estimated in Table 4.2 when using the the reference processes (R1)-(R3) (from the left to the right). The solid lines show the densities of the typical radius under the corresponding reference processes.

interaction models from Table 4.2, let $n = 10^6$ be the number of MCMC iterations, and the i-th iteration, k_i denotes the number of discs, $r_j^{(i)}$ the radius of the j-th disc in the i-th iteration, and

$$F_i(r) = \frac{1}{k_i} \sum_{j=1}^{k_i} \mathbb{I}_{[r_j^{(i)} \leq r]}$$

the empirical distribution function of the radii. The histogram in Figure 4.3 is then obtained from the average of empirical distribution functions as

$$\bar{F}(r) = \frac{1}{n} \sum_{i=1}^{n} F_i(r)$$

which may be interpreted as an estimate of the distribution of a typical radius R under the estimated (A, L, N_{cc})-interaction model.

Remark 4.5 *When we instead considered the average*

$$\tilde{F}(r) = \frac{1}{\sum_{i=1}^{n} k_i} \sum_{i=1}^{n} \sum_{j=1}^{k_i} \mathbb{I}_{[r_j^{(i)} \leq r]},$$

we obtained a very similar distribution, therefore it is not shown in this work.

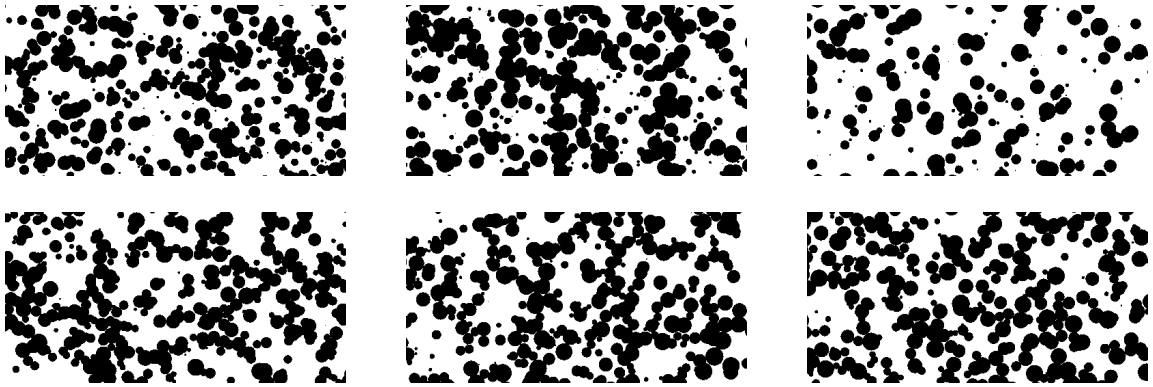

Figure 4.4: Simulations of the Boolean models (R1)-(R3) (upper row from the left to the right) and of the fitted (A, L, N_{cc})-interaction models when using the the reference processes (R1)-(R3) (lower row from the left to the right).

4.6 Model validation

In this section, we consider results for the three fitted (A, L, N_{cc})-interaction models based on the conditional likelihood L_c, but similar conclusions are obtained when instead the unconditional likelihood L_u is considered. For comparison, we also consider how well the Boolean models (R1)-(R3) fit the heather data.

Figure 4.4 shows simulated realizations of the random-disc Boolean models (R1)-(R3) and the fitted (A, L, N_{cc})-interaction models. As expected, because of the too low area fraction, the realization under (R3) looks very different from the others, and the many small connected components obtained under (R1)-(R3) seem less frequent under the fitted (A, L, N_{cc})-interaction models.

Since it is hard to check only visually how well the estimated models fit the heather data, we consider in the sequel different summary statistics specified by various contact distribution functions and covariance function, as usually considered in stochastic geometry, and also shape characteristics obtained by certain operations from mathematical morphology.

In Sections 4.6.1-4.6.2, we consider first a general planar random closed set $\mathbf{Z}$. We naturally specify non-parametric estimates of the summary statistics with edge corrections, where we use a regular quadratic lattice with vertex set G given by the centers of the 250×508 pixels in Figure 4.1.

4.6.1 Contact distribution functions

In the stationary case of $\mathbf{Z}$, a natural non-parametric estimator is given by

$$\hat{H}_B(r) = \frac{\sum_{u \in G} \mathbb{I}_{[u \notin \mathbf{Z},\, u+rB \subset W,\, (u+rB) \cap \mathbf{Z} \neq \emptyset]}}{\sum_{u \in G} \mathbb{I}_{[u \notin \mathbf{Z},\, u+rB \subset W]}} \tag{4.6.1.1}$$

where we have used the border method to correct edge effects and therefore we consider only vertices u with $u + rB \subset W$. As the structuring element B, we use

- a unit line segment with endpoints $(-0.5\cos\varphi, -0.5\sin\varphi)$ and $(0.5\cos\varphi, 0.5\sin\varphi)$, where $0 \leq \varphi < \pi$, and we write H_φ for H_B (the linear contact distribution function),
- a unit disc $b(0,1)$, and write H_s for H_B (the circular/spherical contact distribution function),
- a unit square $[-0.5, 0.5] \times [-0.5, 0.5]$, and write H_q for H_B (the quadratic contact distribution function).

For our random-disc Boolean models,

$$H_B(r) = 1 - \exp\left(-\rho\left(L(B)\mu r + A(B)r^2\right)\right) \tag{4.6.1.2}$$

where $L(B) = 2$ in the case of the linear contact distribution function.

Let

$$T_B(r) = -\frac{1}{r}\log\left(1 - H_B(r)\right), \quad r > 0,$$

and denote $\hat{T}_B(r)$ the non-parametric estimate obtained by replacing $H_B(r)$ by (4.6.1.1). Then (4.6.1.2) implies that

$$T_\varphi(r) = 2\rho\mu, \quad T_s(r) = 2\rho\pi\mu + \rho\pi r, \quad T_q(r) = 4\rho\mu + \rho r. \tag{4.6.1.3}$$

Figure 4.5 compares the theoretical functions $T_B(r)$ given by (4.6.1.3) for respective (R1)-(R3) with $\hat{T}_B(r)$ based on the data and its simulated 2.5% and 97.5% envelopes obtained from 39 simulations under respective (R1)-(R3) and the corresponding three (A, L, N_{cc})-interaction models.

It is seen that none of the Boolean models (R1)-(R3) provide a satisfactory fit, as $T_B(r)$ is below $\hat{T}_B(r)$ with the upper 97.5% envelope close to $\hat{T}_B(r)$ in most cases of (R1)-(R2), while this envelope is much below $\hat{T}_B(r)$ in case of (R3). In contrast Figure 4.5 reveals no problems with any of the three (A, L, N_{cc})-interaction models.

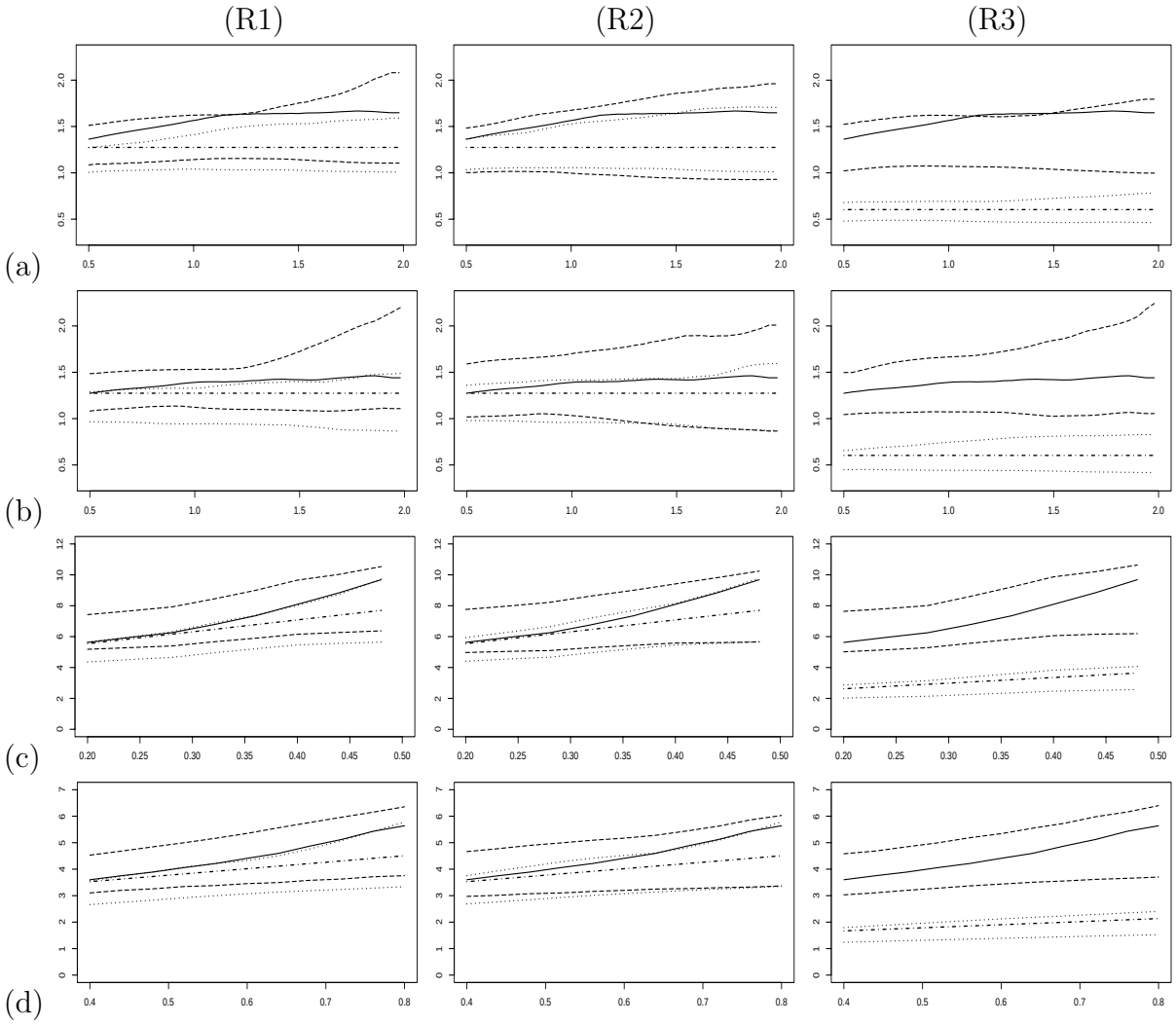

Figure 4.5: Comparing the theoretical functions $T_B(r)$ (dot-dashed lines) with $\hat{T}_B(r)$ (solid lines) based on the data and its simulated 2.5% and 97.5% envelopes obtained under the Boolean model (R1), (R2), or (R3) (dotted lines) and the corresponding (A, L, N_{cc})-interaction model (dashed lines). The three columns correspond from the left to the right to results when (R1), (R2), or (R3) is used either as a fitted model or as a reference process. For the rows, different structuring elements are specified by (a) the line segment with $\varphi = 0$, (b) the line segment with $\varphi = \pi/2$, (c) the unit disc $b(0, 1)$, and (d) the unit square $[-0.5, 0.5] \times [-0.5, 0.5]$.

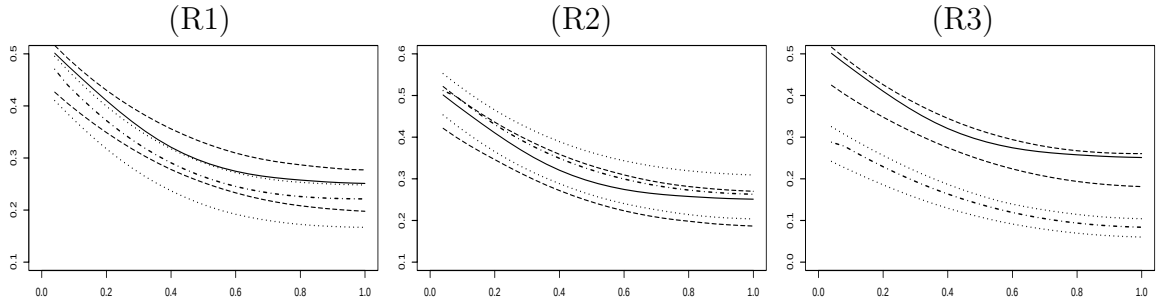

Figure 4.6: Comparing the theoretical functions $C(r)$ (dot-dashed lines) with $\hat{C}(r)$ (solid lines) based on the data and its simulated 2.5% and 97.5% envelopes obtained under the Boolean model (R1), (R2), or (R3) (dotted lines) and the corresponding $(A, L, N_{\rm cc})$-interaction model (dashed lines). The three plots correspond from the left to the right to results when (R1), (R2), or (R3) is used either as a fitted model or as a reference process.

4.6.2 Covariance function

Assuming $\mathbf{Z}$ is motion invariant, an unbiased and edge corrected non-parametric estimator of covariance function based on the border method is given by

$$\hat{C}(r) = \frac{\sum_{u,v\in G} \mathbb{I}_{[\|u-v\|=r,\, \{u,v\}\subset \mathbf{Z}]}}{\sum_{u,v\in G} \mathbb{I}_{[\|u-v\|=r]}} \tag{4.6.2.1}$$

provided the denominator is non-zero.

For a random-disc Boolean model,

$$C(r) = 2p - 1 + (1-p)^2 \exp\left(\rho \mathbb{E}\left[2R^2 \arccos\frac{R}{2r} - \frac{r}{2}\sqrt{4R^2 - r^2}\right]\right) \tag{4.6.2.2}$$

where the expectation may be evaluated by numerical methods.

Figure 4.6 compares the theoretical function $C(r)$ given by (4.6.2.2) and (R1)-(R3) with $\hat{C}(r)$ in (4.6.2.1) based on the data and its simulated 2.5% and 97.5% envelopes obtained under the Boolean models (R1)-(R3) and the corresponding three $(A, L, N_{\rm cc})$-interaction models. The figure reveals no misfit for neither (R2) or any of the three $(A, L, N_{\rm cc})$-interaction models. However, $\hat{C}(r)$ is very close to the 97.5%-envelope obtained for (R1), and there is a clear misfit in case of (R3).

4.6.3 Shape characteristics

This method is based on enlarging and reducing the given set.

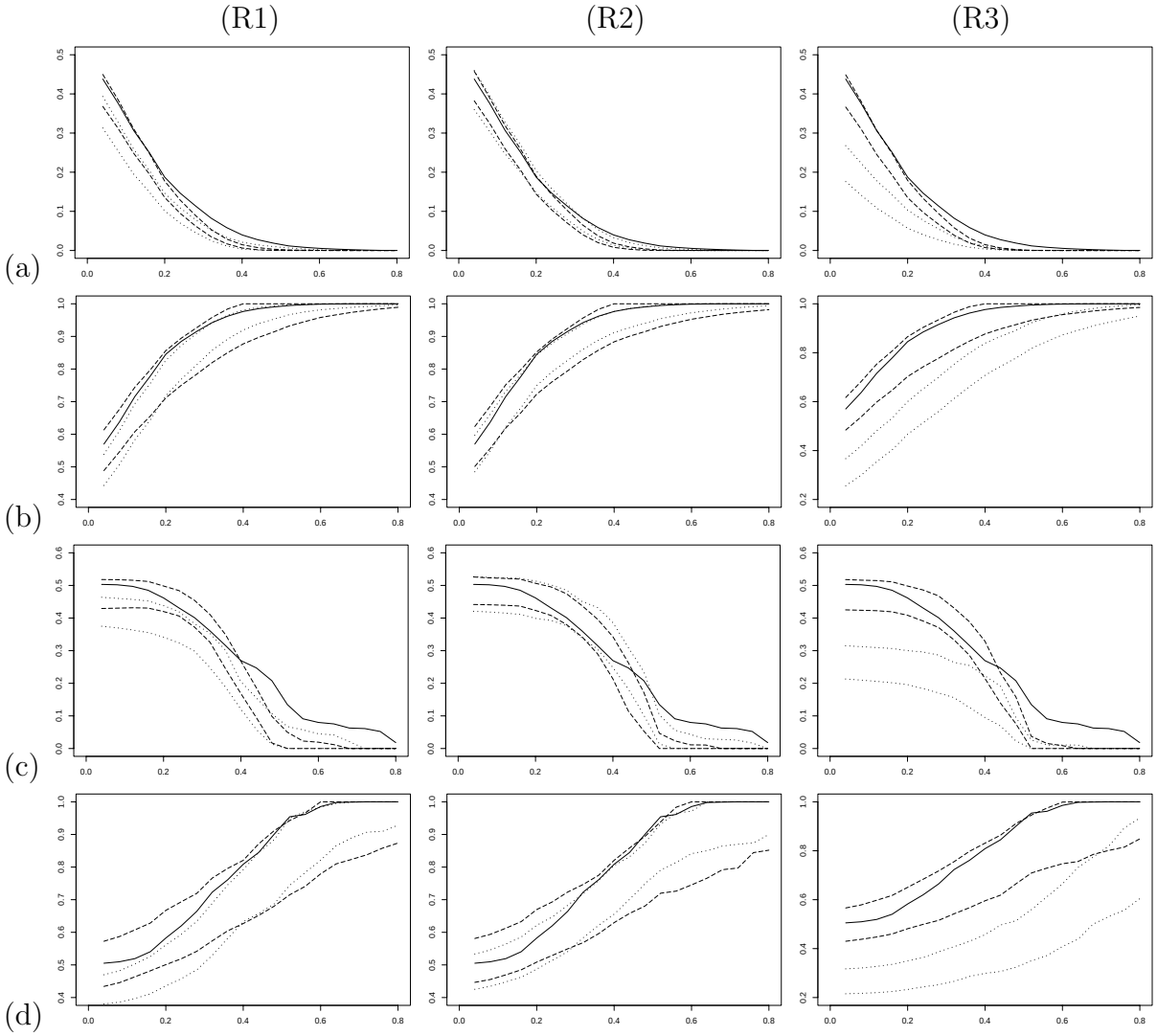

Figure 4.7: Comparing (a) erosion e_r, (b) dilatation d_r, (c) opening o_r, and (d) closing c_r of the heather data set (solid lines) with simulated 2.5% and 97.5% envelopes obtained under the Boolean model (R1), (R2), or (R3) (dotted lines) and the corresponding (A, L, N_{cc})-interaction model (dashed lines). The three columns correspond from the left to the right to results when (R1), (R2) or (R3) is used either as a fitted model or as a reference process.

Here, we describe the shape of $\tilde{\mathbf{Z}} = \mathbf{Z} \cap W$ for any set $\mathbf{Z} \subset \mathbb{R}^2$ as follows. Let $|\mathbf{Z}| = A(\mathbf{Z})$ and for all numbers $r > 0$, let $\mathbf{Z}_{\ominus r} = \{u \in \mathbb{R}^2 : b(u, r) \subseteq \mathbf{Z}\}$, and $\mathbf{Z}_{\oplus r} = \cup_{u \in \mathbf{Z}} b(u, r)$. Erosion e_r, dilation d_r, opening o_r, and closing c_r of $\tilde{\mathbf{Z}}$ by the disc $b(0, r)$ are defined by

$$e_r = \frac{|\tilde{\mathbf{Z}}_{\ominus r}|}{|W_{\ominus r}|}, \quad d_r = \frac{|\tilde{\mathbf{Z}}_{\oplus r} \cap W_{\ominus r}|}{|W_{\ominus r}|}, \quad o_r = \frac{|(\tilde{\mathbf{Z}}_{\ominus r})_{\oplus r} \cap W_{\ominus 2r}|}{|W_{\ominus 2r}|}, \quad c_r = \frac{|(\tilde{\mathbf{Z}}_{\oplus r})_{\ominus r} \cap W_{\ominus 2r}|}{|W_{\ominus 2r}|}. \tag{4.6.3.1}$$

Figure 4.7 compares these shape-characteristics based on the data with simulated 2.5% and 97.5% envelopes obtained under the Boolean models (R1)-(R3) and the corresponding three (A, L, N_{cc})-interaction models. In case of dilation and closing, the figure reveals no clear misfit for neither (R2) or any of the three (A, L, N_{cc})-interaction models, while (R1) and particularly (R3) are not fitting well. Furthermore, in case of erosion and opening, the figure indicates that any of the six models is not fitting well, possibly since the heather data are rather smooth while a disc process is naturally more rugged.

Chapter 5

Software solution

Since there exists no software applicable to the introduced model, we produced our own programs specialized for simulating realizations from a density (3.3.1.2) and (3.3.4.2), when given coefficients $\theta_1, \ldots, \theta_6$ and for estimating the parameters of the density (4.1.0.1) by both conditional and unconditional simulation-based maximum likelihood when given data as well as the programs for consequent model validation introduced in Section 4.6. For obtaining the simulations, we used Metropolis-Hastings algorithm described in Section 3.4.1, where for calculating the Papangelou conditional intensity (3.3.2.1) or (3.3.4.3) it handles with the power tessellation studied in Section 3.2 following the construction method from Section 3.2.2.

The programs which were produced in program language C++ can be found on the enclosed CD. Their main parts and artifices are described in this section.

Remark 5.1 *In C++, loops, arrays, matrices etc. usually start by number 0, for example a vector v of the length k is recorded as $(v[0], \ldots, v[k-1])$. Therefore, when we will for example speak about the i-th disc, we will refer it as a disc number $i-1$.*

5.1 Program "MCMC-simulation.cpp"

This program which simulates realizations from a given density (3.3.1.2), is the base of all introduced programs. It is the most difficult part of software solution and hence, it will be described in the most details.

5.1.1 Inputs and outputs of the program

The input of the program is the specification of the reference Boolean model, the density, the set S of the discs centers and the number of iterations. This specification is done inside the program. A user can choose one of the offered radii distributions (the program includes the uniform and exponential distribution with arbitrary parameters, later, the restricted normal distribution was added into the programs for statistical analysis), set its parameters and determine the (constant) intensity ρ of the reference process. Then, the density is specified by setting the parameters $\theta_1, \ldots, \theta_6$. The set S is rectangular with arbitrary chosen width A and height B. Finally, the specification of the number of iterations is required.

The main aim of the program is to obtain a simulated realization of the disc process, hence the main output of the program is the file "balls.txt" describing the simulated discs, see below. However, since we need to establish the burn-in time as mentioned in Section 3.4, we require further the outputs describing time evolution of the individual geometrical characteristics. Moreover, since we are interested also in the power tessellation corresponding to the simulated disc process, the program produces also outputs describing the tessellation. The complete output is then formed by the following files:

1. Files describing the final realization:
   - "numballs.txt": file containing one number N_b corresponding to the number of discs in the realization;
   - "balls.txt": file containing a matrix of the dimension $N_b \times 3$, where first two columns describe x- and y- coordinates of the centers and the third column determines the radii of the discs in the realization.
2. Files describing evolution of the geometrical characteristics of the union of discs and probability of acceptation during the simulation - each file consists a vector of the length n, where n is the number of iterations of MCMC algorithm, and the i-th item of this vector is equal to the value of the given geometrical characteristic for the union of the discs and probability of acceptation in the i-th iteration:
   - "area.txt": file describing evolution of the area;
   - "perim.txt" file describing evolution of the perimeter;
   - "epchar.txt" file describing evolution of the Euler-Poincaré characteristic;
   - "ncc.txt" file describing evolution of the number of connected components;
   - "nic.txt" file describing evolution of the number of isolated cells;
   - "nbv.txt" file describing evolution of the number of boundary vertices;

- "probacc.txt" file describing evolution of probability of acceptation of a proposal in MCMC algorithm.

3. Files describing the corresponding power tessellation:

   - "noies.txt": file containing one number N_{ie} corresponding to the number of all interior edges in the union;
   - "interedges.txt": file containing a matrix of the dimension $N_{ie} \times 6$, where the first two columns determine the discs defining the edge (e.g. the numbers 0 and 1 means - due to Remark 5.1 - that the edge is produced by the first and the second disc from the file "balls.txt"), the third and the fourth columns correspond to the x- and y-coordinates of one of the endpoints and the last two columns give the coordinates of the second endpoint of the corresponding interior edge;
   - "nobes.txt": file containing one number N_{be} corresponding to the number of all boundary edges in the union;
   - "boundedges.txt": file containing a matrix of the dimension $N_{be} \times 8$, where the first column determines the disc which produces the boundary edge (e.g. 0 means that the edge is a part of the boundary of the first disc from the file "balls.txt"), the second column gives the order number of boundary edges in the frame of the given disc, the third and the fourth column as well as the fifth and the sixth column correspond to the x- and y-coordinates of the first, respective the second, endpoint of the edge (in anti-clockwise order) and the last two columns describe the angles between the horizontal line and the line given by the join between the endpoint and the center of the corresponding disc (these angles are used for drawing the tessellation);
   - "noic.txt": file containing one number N_{ic} corresponding to the number of all isolated cells in the union;
   - "isolcells.txt": file used for drawing the tessellation containing a matrix of the dimension $N_{ic} \times 3$, where two first columns describe x- and y- coordinates of the centers and the third column determines the radius of each of the isolated cells;
   - "limits.txt": file again used for drawing the tessellation containing two numbers min and max such that min corresponds to the value $\min(min_x, min_y)$, where min_x is the minimal value on the x-axe reached by the union and min_y is analogously minimal value on the y-axe (as follows from the fact that the discs may expand outside of the set of their centers S, the value min can be lower then the lower boundary coordinate for the set S) while max is the maximal reached coordinate.

5.1.2 Basic settings and structures

In this section, we describe the implementation of the geometrical objects described in theoretical part of this work in the language C++.

Since we work with discs, we first introduce the constant π as

```
#define pi 3.1415922654
```

used mainly for calculating with disc area and perimeter, and also for the work with angles as described in Section 3.2.2.

Further, we define a generator of a random value from uniform distribution on the interval $[0, 1]$ as

```
#define MY_RAND() (float)rand()/RAND_MAX
```

based on generating a random positive integer between 0 and 2^8 and dividing it by the value 2^8. A random value from another probability distribution is then derived by a transformation (based on the corresponding distribution function) of the value obtained from this generator.

To build a structure of the power tessellation, we need two more constants

```
#define maxb 1000
#define maxv 100
```

defining upper bound for the number of discs in the simulated union and for the number of neighboring discs for each disc, respectively. Moreover, in order to build the tessellation structure as well-arranged as possible, we introduce the following structures:

- a point given by its two coordinates

  ```
  typedef struct {float coor1; float coor2;} POINT;
  ```

- a disc given by its center and its radius

  ```
  typedef struct {POINT centre; float radius;} BALL;
  ```

- a vertex

  ```
  typedef struct {int type; POINT point;} VERTEX;
  ```

  as a special point which can be of the type 0 when it is an interior vertex of the tessellation, 1 in the case of a boundary vertex, or 2 when it is not exactly a vertex of the tessellation, but only the point denoting the identical endpoints of the boundary edge in the case of an isolated cell;

- an interior edge

  ```
  typedef struct {int nonempty; VERTEX endp1; VERTEX endp2;} INTEDGE;
  ```

  given by its endpoints introduced in arbitrary order and by the item `nonempty` which can acquire either the value 0 in the case it is empty or the value 1 if it is nonempty;

- a boundary edge

  ```
  typedef struct {int nobe; VERTEX endp1[maxv]; VERTEX endp2[maxv];}
  BEDGE;
  ```

  given by its endpoints ordered anti-clockwise which are moreover marked by the number denoting its order in the frame of the concerned cell (e.g. `endp1[2]` denotes the first endpoint of the third boundary edge belonging to the same cell) and `nobe` denotes the number of all boundary edges belonging to the concerned cell.

The structure of the power tessellation is the main structure in the program. It is defined so that it allows us to recalculate all the geometrical characteristics of the union for both cases when a disc is added or deleted, respectively. Its implementation is the following:

```
typedef struct
   {
    int nb; BALL ball[maxb];
    INTEDGE ie[maxb][maxb]; int noie[maxb]; int noies;
    BEDGE be[maxb]; int nobes;
    float aoc[maxb]; float poc[maxb];
    int neighbors[maxb][maxv]; int noneighb[maxb];
    float area; float perimeter; int epchar; int nh;
    int nic; int nnc; int ncc; int nbv;
   }
TESSEL;
```

where

`nb` denotes the number of discs,
`ie[i][j]` is the interior edge between i-th and j-th disc,
`noie[i]` the number of interior edges of the i-th cell,
`noies` the number of all interior edges in the union,
`be[i]` boundary edges belonging to the i-th disc,
`nobes` the number of all boundary edges,
`ball[i]` i-th disc of the union,
`aoc[i]` the area of the i-th cell,
`poc[i]` total length of boundary edges of the i-th cell,
`neighbors[i][j]` the j-the neighboring disc of the i-th disc and
`noneighb[i]` the number of discs neighboring with the i-th disc.

Further,

`area` is the total area,
`perimeter` the total perimeter,
`epchar` the Euler-Poincaré characteristic,
`nh` the number of holes,
`nic` the number of isolated cells,
`nnc` the number of nonempty cells,
`ncc` the number of connected components and
`nbv` the number of boundary vertices

of the tessellation.

5.1.3 Program structure

The program consists of many small functions and procedures included to bigger ones. Then, the main part consist of one for-loop using only two main procedures which calculates the changes of the edges and the geometrical characteristics of the new tessellation when a disc is added or deleted and which tightly follow the algorithm described in Section 3.2.2. It would be useless and unnoticed to describe all the functions and procedures in details, therefore, we show the idea of the program by describing only the two procedures and consequently the structure of the main program.

Procedure "add_new_ball"

Input of this procedure is the old tessellation represented by the structure `TESSEL` as described above and a newly added disc represented by two coordinates and a radius chosen randomly during running the program so that it follows the proposal density. Output of this procedure is again a structure TESSEL representing the tessellation with the added disc. Note that because of the size of the remembered values, the procedure works with pointers denoted by "*". Thus, the frame of the procedure is following:

```
TESSEL *add_new_ball (TESSEL *tessel,float ballcoor1, float ballcoor2,
float ballradius)
{
  ...
  return (tessel);
}
```

Probably the main artifice is to keep track on the groups of neighboring discs represented by `neighbors[i][j]` and on the number of neighbors of the $i+1$-th disc `noneighb[i]` in the structure TESSEL. In fact, it is the representation of the dual graph (with the difference that it remembers also the discs which produce empty cells), i.e. it is the tool which allows us to make the local calculations as mentioned in Section 3.4.2 which make the program much faster, because we focus only on the discs which are intersected by the newly added disc.

The procedure itself then work in the following steps:

1. A new disc is added to the old tessellation:

   ```
   tessel->ball[tessel->nb].centre.coor1=ballcoor1;
   tessel->ball[tessel->nb].centre.coor2=ballcoor2;
   tessel->ball[tessel->nb].radius=ballradius;
   ```

2. The items which keep track on neighboring discs are changed using a special function which add the new disc to the lists of neighbors for all intersected discs and moreover write these discs to the list of neighbors for the added disc:

   ```
   tessel=build_neighbors_add_ball(tessel,tessel->nb);
   ```

3. The number of the interior and boundary edges, the area and the perimeter of the cells which are intersected by the newly added disc are subtracted:

```
tessel->noies=tessel->noies*2;
for (i=0;i<tessel->noneighb[tessel->nb];i++)
  {
   if (type_of_cell(tessel,tessel->neighbors[tessel->nb][i])==1)
     {
      tessel->nnc--;
     }
   if (type_of_cell(tessel,tessel->neighbors[tessel->nb][i])==2)
     {
      tessel->nnc--;tessel->nic--;
     }
   tessel->noies
    =tessel->noies-tessel->noie[tessel->neighbors[tessel->nb][i]];
   tessel->nobes
    =tessel->nobes-tessel->be[tessel->neighbors[tessel->nb][i]].nobe;
   tessel->area
    =tessel->area-tessel->aoc[tessel->neighbors[tessel->nb][i]];
   tessel->perimeter
    =tessel->perimeter-tessel->poc[tessel->neighbors[tessel->nb][i]];
  }
```

4. The new tessellation is produced by building the interior and boundary edges for the part of the tessellation which was changed by a newly added disc. It is done so that first, the chords between two discs are considered to be a new interior edge (function "new_chords"), then the line is reduced (function "repair_chords") as described by (iii) from the algorithm in Section 3.2.2, and finally the boundary edges of all changed cells are recalculated (function "repair_bound") following together (iv) and (v) from the algorithm in Section 3.2.2:

```
tessel=new_chords(tessel,tessel->nb);
for (i=0;i<tessel->noneighb[tessel->nb];i++)
  {
   tessel=new_chords(tessel,tessel->neighbors[tessel->nb][i]);
  }
tessel=repair_chords(tessel,tessel->nb);
for (i=0;i<tessel->noneighb[tessel->nb];i++)
  {
   tessel=repair_chords(tessel,tessel->neighbors[tessel->nb][i]);
  }
tessel=repair_bound(tessel,tessel->nb);
for (i=0;i<tessel->noneighb[tessel->nb];i++)
  {
```

```
   tessel=repair_bound(tessel,tessel->neighbors[tessel->nb][i]);
  }
```

5. The new values of the area and the perimeter of the cells which are intersected by the newly added disc are calculated:

```
for (i=0;i<tessel->noneighb[tessel->nb];i++)
  {
   tessel->aoc[tessel->neighbors[tessel->nb][i]]
    =area_of_cell(tessel,tessel->neighbors[tessel->nb][i]);
   tessel->poc[tessel->neighbors[tessel->nb][i]]
    =perim_of_be_of_cell(tessel,tessel->neighbors[tessel->nb][i]);
  }
```

6. The other characteristics of cells which are intersected by the newly added disc are calculated:

```
for (i=0;i<tessel->noneighb[tessel->nb];i++)
  {
   if (type_of_cell(tessel,tessel->neighbors[tessel->nb][i])==1)
     {
      tessel->nnc++;
     }
   if (type_of_cell(tessel,tessel->neighbors[tessel->nb][i])==2)
     {
      tessel->nnc++;tessel->nic++;
     }
   tessel->noies
    =tessel->noies+tessel->noie[tessel->neighbors[tessel->nb][i]];
   tessel->nobes
    =tessel->nobes+tessel->be[tessel->neighbors[tessel->nb][i]].nobe;
   tessel->area
    =tessel->area+tessel->aoc[tessel->neighbors[tessel->nb][i]];
   tessel->perimeter
    =tessel->perimeter+tessel->poc[tessel->neighbors[tessel->nb][i]];
  }
```

7. The area and the perimeter of the new cell are calculated:

```
tessel->aoc[tessel->nb]=area_of_cell(tessel,tessel->nb);
tessel->poc[tessel->nb]=perim_of_be_of_cell(tessel,tessel->nb);
```

8. New characteristics of the whole tessellation are calculated:

```
if (type_of_cell(tessel,tessel->nb)==1)
  {
   tessel->nnc++;
  }
if (type_of_cell(tessel,tessel->nb)==2)
  {
   tessel->nnc++;tessel->nic++;
  }
tessel->noies=tessel->noies+tessel->noie[tessel->nb];
tessel->noies=tessel->noies/2;
tessel->nobes=tessel->nobes+tessel->be[tessel->nb].nobe;
tessel->area=tessel->area+tessel->aoc[tessel->nb];
tessel->perimeter=tessel->perimeter+tessel->poc[tessel->nb];
tessel->epchar=tessel->nnc - tessel->noies
 +(tessel->noies+tessel->nobes-tessel->nic)*2/3
 -(tessel->nobes-tessel->nic);
tessel->nb++;
tessel->ncc=Number_of_connected_components(tessel);
tessel->nbv=tessel->nobes-tessel->nic;
```

Procedure "delete_nth_ball"

Input of this procedure is again the old tessellation represented by the structure `TESSEL` and an integer `n` meaning that the $(n+1)$-th disc should be deleted. As well as in the previous procedure, output of the procedure is the structure of the tessellation without the deleted disc.

The main artifice is again in the part when the items describing the neighboring disc are changed. Here, it is done in two steps. First, the disc which should be deleted, is omitted from the array of the discs intersected by it, so it is not their neighbor any more:

```
for (i=0;i<tessel->noneighb[n];i++)
    {
     for (j=0;(tessel->neighbors[tessel->neighbors[n][i]][j]!=n)
          &&(j<tessel->noneighb[tessel->neighbors[n][i]]);j++)
       {
        tessel->noneighb[tessel->neighbors[n][i]]--;
        tessel->neighbors[tessel->neighbors[n][i]][j]
```

```
        =tessel->neighbors[tessel->neighbors[n][i]]
                          [tessel->noneighb[tessel->neighbors[n][i]]];
      }
    }
```

Secondly, the orders of discs are recalculated so that the last disc (i.e. `ball[nb-1]`) is removed to the place of the deleted disc in order not to have empty space disc instead of the deleted disc (it is easier and faster than renumbering all discs `ball[n+1]`, `ball[n+2]`,...,`ball[nb-1]`):

```
tessel->nb--;
if (tessel->nb!=n)
  {
   tessel->ball[n]=tessel->ball[tessel->nb];
   for (i=0;i<tessel->noneighb[tessel->nb];i++)
     {
      tessel->ie[n][tessel->neighbors[tessel->nb][i]]
       =tessel->ie[tessel->nb][tessel->neighbors[tessel->nb][i]];
      tessel->ie[tessel->neighbors[tessel->nb][i]][n]
       =tessel->ie[tessel->neighbors[tessel->nb][i]][tessel->nb];
     }
   tessel->be[n]=tessel->be[tessel->nb];
   tessel->noie[n]=tessel->noie[tessel->nb];
   tessel->aoc[n]=tessel->aoc[tessel->nb];
   tessel->poc[n]=tessel->poc[tessel->nb];
  }
   for (i=0;i<tessel->noneighb[tessel->nb];i++)
     {
      tessel->neighbors[n][i]=tessel->neighbors[tessel->nb][i];
     }
   tessel->noneighb[n]=tessel->noneighb[tessel->nb];
   for (i=0;i<tessel->noneighb[n];i++)
     {
      for(j=0;
          (tessel->neighbors[tessel->neighbors[n][i]][j]!=tessel->nb)
          &&(j<tessel->noneighb[tessel->neighbors[n][i]]);j++)
        {
         tessel->neighbors[tessel->neighbors[n][i]][j]=n;
        }
     }
```

All the remaining steps calculating the endpoints of the edges and the geometrical

characteristics are analogous to that ones introduced when describing the procedure `add_new_disc`.

The main part of the program

Having the procedures described above, the main program is then short and easily comprehensible, since it strictly follows the Metropolis-Hastings algorithm from Section 3.4.1

As an example, we show its structure in the case when we simulate from the density (3.3.1.2) with respect to the process of discs with radii distributed uniformly in the interval $[0, 2]$, centers in the rectangular window with side lengths $A \times B$ and probability p of adding a disc. Note that the value `noiter` in the program denotes the number of iterations.

```
for (i=0;i<noiter;i++)
 {
  u1=MY_RAND();
  if (u1<p) //proposal of adding a disc
    {
     *helptessel=*tessel;
     helptessel=add_new_ball (helptessel,A*MY_RAND(),B*MY_RAND(),
                              2*MY_RAND());
     papang=exp(theta1*(helptessel->area-tessel->area)
            +theta2*(helptessel->perimeter-tessel->perimeter)
             +theta3*(helptessel->epchar-tessel->epchar)
            +theta4*(helptessel->nh-tessel->nh)
            +theta5*(helptessel->nic-tessel->nic)
            +theta6*(helptessel->nbv-tessel->nbv));
     h=papang*A*B*rho/(helptessel->nb);
     u2=MY_RAND();
     if (u2<h) //proposal accepted
       {
        *tessel=*helptessel;
       }
    }
  else //proposal of deleting a disc
    {
     *helptessel=*tessel;
     n=(int)(MY_RAND()*helptessel->nb);
     helptessel=delete_nth_ball(helptessel,n);
     papang=exp(-theta1*(helptessel->area-tessel->area)
```

```
          -theta2*(helptessel->perimeter-tessel->perimeter)
          -theta3*(helptessel->epchar-tessel->epchar)
          -theta4*(helptessel->nh-tessel->nh)
          -theta5*(helptessel->nic-tessel->nic)
          -theta6*(helptessel->nbv-tessel->nbv));
 h=papang*A*B*rho/(tessel->nb);
 u2=MY_RAND();
 if (u2<(1/h)) //proposal accepted
   {
    *tessel=*helptessel;
   }
}
```

5.2 Programs for estimating the parameters

When estimating the parameters of the model by both conditional and unconditional likelihood, the program "MCMC-simulation.cpp" is the base. There are no special artifices in the programs for estimating the parameters, as they exactly follow the methods described in the Section 4.3. First, the number of the realizations needed is simulated, and then, the Newton-Raphson method for estimating the parameters is used. However, there are some problems with coordinating a digital image of the data with simulated discs and also with the size of computer memory. Therefore there were added some modifications and procedures which are described in this section.

5.2.1 Program "MCMC-MLE_conditional_full_model.cpp"

This program estimates the parameters in the model (4.1.0.1). As follows from the MCMC maximum likelihood method, input of the program contains the values of the geometrical characteristics of the data and the information about the data components lying on the boundary of the observation window. This information is obtained in the input file "heather_V.txt" which is a 250×508 matrix of numbers 0,1 and 2 corresponding to white pixels (i.e. places out of the heather grow), black pixels (i.e. the heather components completely contained in the observation window) and gray pixels (i.e. the components intersecting the boundary of the observation window), respectively, from the Figure 4.2. Since for the conditional likelihood we need only the realizations of the discs which intersect neither the boundary of the observation window nor the gray components we have to add a procedure into the program which checks whether a disc can be added (then it returns the value 1) or not (the returned value is 0). When doing so, discs are translated into a digital representation so that a pixel forms a disc if the point in $\mathbb{R}^2$

corresponding to the center of the pixel is included in the given disc. Input of the function is a matrix `mat` given in our case by the input file "heather_V.txt" and its implementation is the following:

```
int accept_ball (MATRIX mat, float A, float B,
float ballcoor1, float ballcoor2, float ballradius)
{
  int r, coor1, coor2, m, n, ok;
  ok = 1;
  if (ballcoor1 < ballradius || ballcoor2 < ballradius ||
      A-ballcoor1 < ballradius || B-ballcoor2 < ballradius)
    {
     ok = 0;
    }
  else
    {
     coor1 = (int)trunc(ballcoor1*25);
     coor2 = (int)trunc(ballcoor2*25);
     r = (int)trunc(ballradius*25) + 1;
     for (m=0; m<2*r; m++)
       {
        for (n=0; n<2*r; n++)
          {
           if ((-r+m)*(-r+m)+(-r+n)*(-r+n)<=r*r &&
               mat.a[coor2-r+m][coor1-r+n]==2)
             {
              ok = 0;
             }
          }
       }
    }
  return (ok);
}
```

Then this function is added at the beginning of the procedure `add_new_ball` as a condition

```
if (accept_ball(mat, A, B, ballcoor1, ballcoor2, ballradius) == 1)
  {
   ...
  }
```

which ensures that the disc is added only in the allowed cases.

The other complication is the fact that the model density is in exponential form and therefore, as follows from (4.3.0.6) and (4.3.0.8), the estimated parameters $\hat{\theta}^{(k)}$ cannot be far away from the initial parameter θ_0, because in the case when the distance between iterated and initial parameters is too large, overflow of the memory could occur. This lead us to include the following procedure:

```
if (dist_of_thetas(theta1est[k], theta2est[k], theta3est[k],
    theta4est[k], theta1, theta2, theta3, theta4) > 2)
  {
   distthetas = dist_of_thetas(theta1est[k], theta2est[k], theta3est[k],
    theta4est[k], theta1, theta2, theta3, theta4);
   theta1est[k] = new_theta(theta1est[k],theta1,distthetas);
   theta2est[k] = new_theta(theta2est[k],theta2,distthetas);
   theta3est[k] = new_theta(theta3est[k],theta3,distthetas);
   theta4est[k] = new_theta(theta4est[k],theta4,distthetas);
  }
```

where `theta1est[k]`,..., `theta4est[k]` represent the items of the parameter vector $\hat{\theta}^{(k)}$, `theta1`,... `theta4` represent the items of the parameter θ_0, the function `dist_of_thetas` calculates the usual Euclidean distance between two points in $\mathbb{R}^4$, the value 2 which is the distance compared to, was chosen experimentally and the function `new_theta` reduces the values `theta1est[k]`,..., `theta4est[k]` so that the new values lie on the intersection of the four-dimensional sphere with radius 2 and the line with endpoints `(theta1est[k],...,theta4est[k])` and `(theta1,...,theta4)`.

5.2.2 Corrections in programs for estimating the parameters in reduced model and for unconditional MCMC MLE

In comparison to the program "MCMC-MLE_conditional_full_model.cpp", only small modifications are needed to be done in the programs

- "MCMC-MLE_conditional_reduced_model.cpp"
- "MCMC-MLE_unconditional_full_model.cpp"
- "MCMC-MLE_unconditional_reduced_model.cpp"

used for estimating the parameters by conditional likelihood in the reduced model and for estimating the parameters by unconditional likelihood in both full and reduced model, re-

spectively. The changes in the case of reduced model are such that the function which calculates the distance between $\hat{\theta}^{(k)}$ and θ_0 is modified for calculating with three-dimensional vectors and that the inputs (geometrical characteristics of the data and initial parameter θ_0) as well as the outputs (estimated parameters) are also three-dimensional. In the programs for estimating based on unconditional likelihood, the only change is omitting the condition

```
if (accept_ball(mat, A, B, ballcoor1, ballcoor2, ballradius) == 1)
```

in the procedure `add_new_ball`, as the acceptance of simulated discs does not depend on the data components intersecting the boundary.

5.3 Programs for model validation

5.3.1 General description

In order to produce the plots shown in Figures 4.5-4.7, we have two programs for each of the introduced summary statistics and shape characteristics - the first one for estimating the given statistic from the data and the second one for establishing the 95% envelopes. These programs are:

- "contact_distribution_function_data.cpp"
- "contact_distribution_function_model.cpp"
- "covariance_function_data.cpp"
- "covariance_function_model.cpp"
- "shape_statistics_data.cpp"
- "shape_statistics_model.cpp"

For easier description of these programs, we introduce the notation $\mathcal{M}$ for the set of all 250×500-dimensional matrices with elements 0 and 1. Here, such matrices are used to describe binary images so that the elements 1 correspond to the black pixels of the image, i.e. to the places belonging to the displayed set, while the elements 0 denote the empty places displayed by white pixels. Further, we use the notation $S(r)$ when generally speaking about the summary statistics and shape characteristics, i.e. $S(r)$ denotes the covariance function, the T-function, dilatation, erosion, opening or closing.

Since in the case of deriving the envelopes we need to produce 39 simulations of the model, we again use the program "MCMC-simulation.cpp" which is modified so that for all the estimated statistics, it works in the following four steps:

1. We obtain 39 independent realizations of the model. All these simulations are produced in a larger window than the observation window W and consequently, only the slice of each simulation which belongs to W is taken into account.

2. We use the added procedure `make_mat` which transforms the 39 simulated unions of discs represented by coordinates of the disc centers and values of the corresponding radii to the matrices $M^{(k)} \in \mathcal{M}$, $k = 1, \ldots, 39$, corresponding to the binary images of the realizations. It is done so that the element $M^{(k)}_{i,j} = 1$ if and only if the point $c \in \mathbb{R}^2$ corresponding to the center of the $[i, j]$-th pixel belongs to the union of simulated discs, i.e. analogously as described in the procedure `accept_ball` in Section 5.2.1.

3. For each of the 39 simulations, we calculate the given statistic $S^{(k)}(r)$, $k = 1, \ldots, 39$, for some sequence of values $\{r_1, ...r_n\}$ simply by counting the number of the elements 1 and 0 in the matrix $M^{(k)}$, $k = 1, \ldots, 39$, due to the relations (4.6.1.1), (4.6.2.1) and (4.6.3.1). The difference between two neighboring values r_i and r_{i+1} is equal to 0.04 m which follows from the fact that one pixel of the image corresponds to the square with the side length 0.04 m.

4. For each of the value $r_i, i = 1, \ldots, n$, we use an easy for-loop to search for the envelopes $\min_{k=1,...,39} S^{(k)}(r_i)$ and $\max_{k=1,...,39} S^{(k)}(r_i)$ of the given statistic S.

When estimating the statistics from the data, the calculating process is much easier, since we need neither to simulate any realizations nor to transform point coordinates and radii to the digital record. The only procedure which is needed is to transform the image from Figure 4.1 to the matrix $M_{heather} \in \mathcal{M}$. Then we work with this matrix as described in the point 3. above.

5.3.2 Special procedures for shape characteristics

Two more special procedures are needed when calculating the values of shape characteristics. Since we work with enlarged and reduced sets, we introduce the procedures `add_pixels` and `del_pixels` which enlarge and reduce, respectively, a set represented as a matrix $M \in \mathcal{M}$ by a "disc" with radius equal to some n-multiple of the pixel size. Inputs of these procedures are the matrix M representing the original set and positive integer n, the output gives the transformed matrix $\tilde{M} \in \mathcal{M}$.

For example the procedure `add_pixels` works so that for each element 1 in the matrix M, all the values in the concerned surroundings (defined again through the centers of the corresponding pixels) are denoted as 1. It is implemented as follows:

```
for (i=0; i<nrow; i++)
  {
   for (j=0; j<ncol; j++)
     {
      if (mat->a[i][j]==1)
        {
         newmat->a[i][j]=1;
         for (k=0; k<2*n+1; k++)
           {
            for (l=0; l<2*n+1; l++)
              {
               if (i-n+k>0 && i-n+k<nrow && j-n+l>0 && j-n+l<ncol
                   && (-n+k)*(-n+k)+(-n+l)*(-n+l)<=n*n)
                 {
                  newmat->a[i-n+k][j-n+l] = 1;
                 }
              }
           }
        }
     }
  }
```

where `nrow` and `ncol` are the numbers of rows and columns of the matrix, and `mat` and `newmat` denotes the original and modified matrix, respectively. The procedure `del_pixels` then works analogously, only with exchanged the values 1 and 0.

5.3.3 Inputs and outputs

Inputs of the programs do not depend on which statistic or characteristic do we estimate, but only on whether we consider the data or the model. While we set only the parameters of the model density together with specification of the reference process when working with the model, in the case of dealing with the data, the input file "heather.txt" which includes the matrix $M_{heather} \in \mathcal{M}$ corresponding to the binary image from Figure 4.1 is needed.

Remark 5.2 *In fact, the dimension of this matrix is not* 250×500*, but* 250×508 *as*

corresponds to the digital image of Figure 4.1. However, when deriving the estimates, we ignore this small difference.

Structure of the outputs again depends on whether we work with the data or with the model. While for the data we get the files with one column of the values of the given estimates for a considered sequence of values $\{r_1, ...r_n\}$, the output files for the model estimates include two columns corresponding to the lower and upper envelopes. The concrete outputs are described in the following paragraphs.

The case of T-function (normalized logarithm of contact distribution function)

For both programs "contact_distribution_function_data.cpp" and "contact_distribution_function_model.cpp", the output is formed by four .txt files consisting of 50 values of T-function (25 values for the spherical T-function, respectively), where the i-th value corresponds to the value in $r = i \cdot 0.04$ m, $i = 1, \ldots, 50$. Each file contains the values for different testing elements, namely

- "Tphi1_heather.txt" and "Tphi1_model.txt" for horizontal line as the testing element,
- "Tphi2_heather.txt" and "Tphi2_model.txt" for vertical line as the testing element,
- "Ts_heather.txt" and "Ts_model.txt" for unit ball as the testing element,
- "Tq_heather.txt" and "Tq_model.txt" for unit square as the testing element.

The case of covariance function

The programs "covariance_function_data.cpp" and "covariance_function_model.cpp" returns the files

- "C_heather.txt" and "C_model.txt"

consisting of 25 values of covariance function in $r = i \cdot 0.04(\text{m})$, $i = 1, \ldots, 25$.

The case of shape characteristics

The programs "shape_statistics_data.cpp" and "shape_statistics_model.cpp" produce on output four files corresponding to the different characteristics, i.e.

- "dilatation_heather.txt" and "dilatation_model.txt"
- "erosion_heather.txt" and "erosion_model.txt"
- "opening_heather.txt" and "opening_model.txt"
- "closing_heather.txt" and "closing_model.txt"

with 20 values of shape statistics in points $r = i \cdot 0.04(\mathrm{m})$, $i = 1, \ldots, 20$.

Chapter 6

Conclusion

In this work, we first provided a description of a model given by a parametric density (with respect to a reference Boolean model) in an exponential family form, where the density was specified by various geometric characteristics of the union of discs. We defined the power tessellation as a useful tool for deriving many of the probabilistic results and geometrical properties of the union as well as for the MCMC simulation of the model.

Secondly, we discussed a statistical analysis of Diggle's heather dataset by fitting the model to it. Results based on two likelihood functions using Markov chain Monte Carlo methods were compared. One of these likelihood functions (the conditional likelihood) was based on a certain conditional distribution such that a spatial Markov property ensured that edge effects were taken into account, while the other likelihood function (the unconditional likelihood) ignored the appearance of discs outside the observation window. We argued that the conditional likelihood was more suitable for statistical inference. Moreover, we compared the results obtained under different fitted Boolean models which were also used as the reference processes when specifying the different interacting disc processes. A model validation based on various summary statistics and simulations showed that the models which include interactions among the discs provide a much better fit than the Boolean models. While our conclusions for the model validation of the various fitted disc process models with interaction did not depend much on which reference processes were used, results for the radii distribution and the intensity of discs were sensitive to the choice of the reference process.

Finally, we explain the software solution of the model analysis and show the main parts of the programs which we developed in order to obtain the introduced results.

Even though the model is evidently usable for description of many events, it is obvious that it can be further generalized. Therefore, we conclude this work with some remarks on possible extensions:

- For the specification of the statistic T in (3.3.1.1), other geometric characteristics may be of interest to include, e.g. shape characteristic such as A/L^2.
- We focus on the case of discs in $\mathbb{R}^2$, however, many results can be extended to the general case of balls in $\mathbb{R}^d$, e.g. $d = 3$ which is important in physics or biology.
- Also extensions of the T-interaction models to infinite configurations of discs would be interesting, especially for applications in statistical physics. Such an extension for quermass-interaction using a local specification can be found e.g. in [5].
- As mentioned in Chapter 4, the radii distribution of the model given by a density with respect to a Boolean model obviously depends on that reference process. It could be studied whether it is possible to find a "limit" radii distribution which would be the same for both the obtained model and the reference process.
- The union of discs can be viewed as a marked point process where the centers of the discs form a spatial point process in plane and the marks are given by the discs radii. Such a spatial marked point process then probably can be extended to a spatio-temporal marked point process.
- The final natural task is how do the properties of the model change in the case when more general random sets are considered instead of discs.

Bibliography

[1] Aurenhammer F. (1987) *Power diagrams: properties, algorithms and applications.* SIAM Journal on Computing **16**, 78 – 96.

[2] Baddeley A. and Møller J. (1989) *Nearest-neighbour Markov point processes and random sets.* International Statistical Review **2**, 89 – 121.

[3] Cressie N.A.C. (1993) *Statistics for Spatial Data.* Wiley, New York.

[4] Diggle P.J. (1981) *Binary mosaics and the spatial pattern of heather.* Biometrics **37**, 531 – 539.

[5] Dereudre D. (2009) *Existence of Quermass-interaction process for non locally stable interaction and non bounded convex grains.* Advances in Applied Probability, accepted.

[6] Edelsbrunner H. (1995) *The union of balls and its dual shape.* Discrete Computational Geometry **13**, 415 – 440.

[7] Hall P. (1985) *Counting methods for inference in binary mosaics.* Biometrics **41**, 1049 – 1052.

[8] Hall P. (1988) *Introduction to the Theory of Coverage Processes.* Wiley, New York.

[9] Häggström O., van Lieshout M.N.M., Møller J. (1999) *Characterization results and Markov chain Monte Carlo algorithms including exact simulation for some spatial point processes.* Bernoulli **5**, 641 – 659.

[10] Herout P. (2004) *Učebnice jazyka C - 1. a 2. díl.* Kopp, České Budějovice. [In Czech]

[11] Kendall W.S., van Lieshout M.N.M., Baddeley A.J. (1999) *Quermass-interaction processes: conditions for stability.* Advances in Applied Probability **31**, 315 – 342.

[12] Laslett G.M., Cressie N., Liow S. (1985) *Intensity estimation in a spatial model of overlaping particles.* Unpublished manuscript, Division of Mathematics and Statistics, CSIRO, Melbourne.

[13] Molchanov I. (1997) *Statistics of the Boolean Model for Practitioners and Mathematicians.* Wiley, Chichester.

[14] Møller J., Helisová K. (2008) *Power diagrams and interaction processes for unions of discs.* Advances in Applied Probability **40**, 321 – 347.

[15] Møller J., Helisová K. (2009) *Likelihood inference for unions of interacting discs.* Scandinavian Journal of Statistics, to appear.

[16] Møller J., Waagepetersen R.P. (2004) *Statistical Inference and Simulation for Spatial Point Processes.* Chapman and Hall/CRC, Boca Raton.

[17] Mrkvička T., Rataj J. (2008) *On estimation of intrinsic volume densities of stationary random closed sets.* Stochastic Processes and Their Applications **118**, 213 – 231.

[18] Ripley B.D. (1988) *Statistical Inference for Spatial Processes.* Cambridge University Press, Cambridge.

[19] Stoyan D., Kendall W.S., Mecke J. (1995) *Stochastic Geometry and Its Applications.* Wiley, Chichester.

[20] Wilson, R. (1972) *Introduction to the Graph Theory.* Oliver and Boyd, Edinburgh.